Scenario Choice Impacts Carbon Allocation Projection at Global Warming Levels

Lee de Mora[1], Ranjini Swaminathan[2], Richard P. Allan[2], Jeremy Blackford[1], Douglas I. Kelley[3], Phil Harris[3], Chris D. Jones[4], Colin G. Jones[5], Spencer Liddicoat[4], Robert J. Parker[6,7], Tristan Quaife[2], Jeremy Walton[4], and Andrew Yool[8]

[1]Plymouth Marine Laboratory, Plymouth, PL1 3DH
[2]National Centre for Earth Observation and Department of Meteorology, University of Reading, Reading, UK
[3]UK Centre for Ecology & Hydrology, Wallingford, Oxfordshire, OX10 8BB, UK
[4]Met Office Hadley Centre for Climate Science and Services, Exeter, EX1 3PB, UK
[5]National Centre for Atmospheric Science, UK, and School of Earth and Environment, University of Leeds, Leeds, UK
[6]National Centre for Earth Observation, Space Park Leicester, University of Leicester, Leicester, UK
[7]Earth Observation Science, School of Physics and Astronomy, University of Leicester, UK
[8]National Oceanography Centre, European Way, Southampton, SO14 3ZH, UK

Correspondence: Lee de Mora (ledm@pml.ac.uk)

Abstract.

We show that the distribution of anthropogenic carbon between the atmosphere, land surface and ocean differs with the choice of projection scenario even for identical changes in mean global surface temperature. Warming thresholds occur later in lower CO_2 emissions scenarios and with less carbon in the three main reservoirs than in higher CO_2 emissions scenarios. At 2 °C of warming, the mean carbon allocation differs by up to 62 PgC between scenarios and this is equivalent to approximately six years of our current global total emissions.

The warming response to carbon dioxide, included via the equilibrium climate sensitivity, ECS, directly impacts the global warming threshold exceedance year and hence the carbon allocation. Low ECS models have more total carbon than high ECS models at a given warming level because the warming threshold occurs later, allowing more emissions to accumulate.

At the same warming level, higher CO_2 concentration scenarios have a lower combined ocean and land carbon allocation fraction of the total carbon than lower CO_2 concentration scenarios. These results are important for carbon budgets and mitigation strategies as they impact how much carbon the ocean and land surface could absorb. Carbon budgeting will be key for reducing the impacts of anthropogenic climate change and these findings could have critical consequences for policies aimed at reaching net zero.

Keywords: Climate change, CMIP6, Earth System Models, Carbon Cycle, Carbon Allocation

1 Introduction

The Intergovernmental Panel on Climate Change (IPCC) Sixth Assessment Report reported that the global mean surface air temperature was 1.1°C warmer in the recent decade (2011-2020) than in the pre-industrial era. They found that human

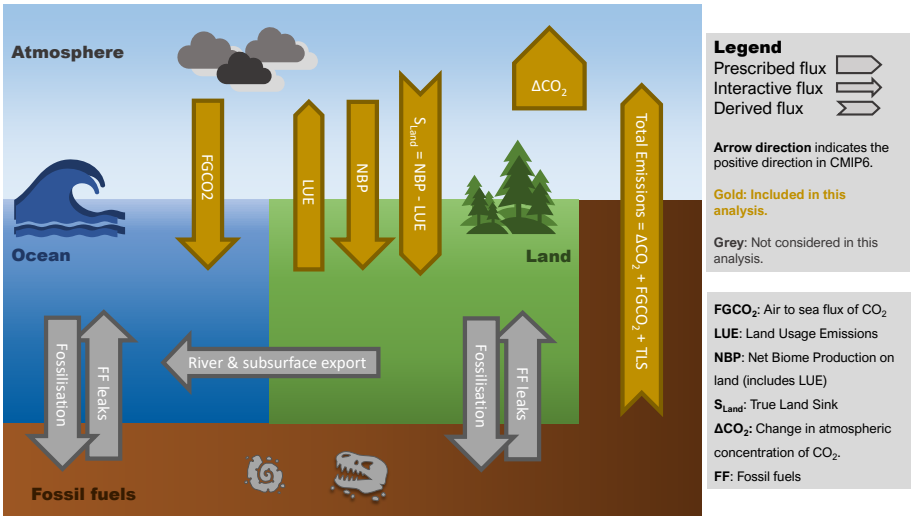

Figure 1. A simplified version of the Earth system carbon cycle. Interactive fluxes are shown as arrows, prescribed fluxes are shown as box arrows, and derived fluxes are shown as chevrons. The arrows in gold are considered in this analysis, and the grey arrows are not considered. The prescribed change in atmospheric carbon, ΔCO_2, accounts for the anthropogenic fossil fuel exploitation and the subsequent carbon emission. Note that while in nature there is a flux of land carbon into the ocean via rivers, and there may be a flux of fossil fuels directly into the ocean or land surface via for instance fossil fuel extraction, these are not generally included in CMIP6 models.

activities have indisputably caused this warming (IPCC, 2021b), with anthropogenic greenhouse gases, particularly carbon dioxide (CO_2), the primary cause.

Since the advent of the industrial revolution, carbon has been transferred gradually from fossil fuel reservoirs to the atmosphere primarily via combustion. Once in the atmosphere, some of the CO_2 is absorbed by the ocean via gas transfer, some is absorbed by the land surface via terrestrial carbon fixation, while some CO_2 remains in the atmosphere, as illustrated in fig. 1. While these fluxes also occur naturally, the additional anthropogenic carbon load has perturbed the Earth system from its pre-industrial equilibrium. In the atmosphere, anthropogenic carbon causes additional warming (Hansen et al., 1981). In the ocean, anthropogenic carbon can cause acidification (Caldeira and Wickett, 2003) or participate in primary production or sequestration (Schlunegger et al., 2019). On the land surface, carbon can allow enhanced primary production and subsequent carbon sequestration. Once converted into biomass, this carbon may be a fuel source in fires (Burton et al., 2022; Sullivan et al., 2022). Through its effect on transpiration rates, elevated atmospheric CO_2 can increase plant growth, impacting flood and drought risk (Ukkola et al., 2016), and worsen food quality and nutrient concentrations (Erda et al., 2005).

The instantaneous distribution of anthropogenic carbon between the atmosphere, ocean and land surface is known as carbon allocation in the Earth system which we define as carbon allocation. The balance between these carbon sinks is hugely important to climate projections and policymakers (IPCC, 2021b), impacting warming feedbacks, marine biogeochemistry and life on land (Macreadie et al., 2019; Hilmi et al., 2021). The physical and biogeochemical feedbacks could affect the future rates of greenhouse gas accumulation in the atmosphere, directly impacting warming (Canadell et al., 2021). They also directly influ-

ence the remaining carbon budget, which policymakers may use to limit fossil fuel consumption in order to keep warming in line with policy goals (Jiang et al., 2021). In addition, the balance of carbon between the atmosphere, land and ocean has large-scale consequences on the future of climate engineering via CO_2 removal and solar radiation modification (Lawrence et al., 2018). Changes to carbon allocation also impact several United Nations Development Programme Sustainable Development Goals, notably 13: Climate Action, 14: Life below Water and 15: Life on Land (United Nations, 2015).

In observations, the atmospheric CO_2 concentration is typically measured directly, while the ocean and terrestrial CO_2 sinks are estimated with global process models constrained by observations. For the decade 2008–2017, the Le Quéré et al. (2018) synopsis of carbon cycle summarised that the fossil fuel emissions were 9.4 ± 0.5 PgC yr^{-1}, and emissions from land use and land-use change was 1.5 ± 0.7 PgC yr^{-1}, most of which was due to deforestation. The growth of the atmospheric carbon was 4.7 ± 0.02 PgC yr^{-1}, the ocean carbon sink was 2.4 ± 0.5 PgC yr^{-1}, and the terrestrial carbon sink was 3.2 ± 0.8 PgC yr^{-1}. In that synthesis, the difference between the estimated total emissions and the estimated changes in the atmosphere, ocean, and terrestrial biosphere was 0.5 PgC yr^{-1}, which indicated that there were either overestimated emissions or underestimated sinks or both. There is a also a flux of land carbon into the ocean via rivers between 0.45 ± 0.18 PgC yr^{-1} and 0.78 ± 0.41 PgC yr^{-1} (Jacobson et al., 2007; Resplandy et al., 2018; Hauck et al., 2020). There may also be a flux of fossil fuels directly into the ocean or land surface via for instance fossil fuel extraction and other leaks (Roser and Ritchie, 2022), but these are not generally included in Earth system models.

It is widely accepted that atmospheric CO_2 is correlated with the global mean atmospheric surface temperature. Figure 5.31 of Canadell et al. (2021) shows the cumulative carbon emissions against global mean temperature change for several projections. That figure shows a strong correspondence between emissions and warming which appears to be scenario independent.

The warming climate and rising atmospheric CO_2 will cause major changes in vegetation structure and function over large fractions of the global land surface. In Friend et al. (2014), an increase in global land vegetation carbon was projected, but with substantial variation between vegetation models. Much of the variability between ESMs in global land vegetation carbon stocks was explained by differences in land vegetation carbon residence time (Jiang et al., 2015). In the ocean, the mechanism is summarised by Katavouta and Williams (2021): an increase in atmospheric CO_2 enhances the ocean carbon storage while warming acts to decrease the ocean carbon storage.

Both the ocean and land carbon sinks are projected to continue to grow as the atmospheric concentration of CO_2 rises (Canadell et al., 2021). However, the combined fraction of emissions taken up by land and ocean is projected to decline, meaning a larger fraction of the emissions remain in the atmosphere. The carbon allocation at the year 2100 is strongly scenario dependent (IPCC, 2021a, fig. SPM7). For instance, in SSP1-1.9, 30% of the carbon remains in the atmosphere in the year 2100, but in SSP5-8.5, that value is 62%. While the land and ocean carbon uptake are expected to remain approximately equal, the uncertainty is much larger for the land carbon sink than the ocean. In the land, some of the uncertainty is due to the balance of increased land carbon accumulation in the high latitudes and loss of land carbon in the tropics (Canadell et al., 2021). Further uncertainty arises from the challenges of forecasting the water cycle, including droughts that reduce carbon absorption potential of the land surface. On the other hand, the ocean CO_2 sink is strongly dependent on the emissions-scenario. This absorption of carbon into the ocean reduces the mean global buffering capacity and drives changes in the global

ocean's carbonate chemistry (Jiang et al., 2019; Katavouta and Williams, 2021). These projections are based on data from the Coupled Model Inter-comparison Project (CMIP), and the most recent CMIP round, CMIP6, is described in sec. 1.1.

1.1 Sixth Coupled Model Inter-comparison Project (CMIP6)

Earth System models (ESMs) are one of the main tools to study the climatic impact of the combustion of fossil fuels, and they are the only tools capable of projecting the future coupled carbon-climate system. The Sixth Coupled Model Inter-comparison Project (CMIP6) (Eyring et al., 2016) is the most recent in a series of global efforts to standardise, share and study ESM simulations. To participate in CMIP6, models must simulate a suite of standard simulations and meet certain model quality and data standards. These standard simulations (also known as the Deck) include a pre-industrial control, a historical simulation, a gradual 1% CO_2 growth experiment and a rapid 4xCO_2 experiment. The quality requirements include a drift in the air-sea flux of CO_2 of less than 10 PgC per century, and a drift in the global volume mean ocean temperature of less than 0.1 degrees per century (Jones et al., 2011; Eyring et al., 2016; Yool et al., 2020).

In order to make projections of the future anthropogenic climate drivers, multiple scenarios were proposed in the ScenarioMIP project to cover a wide range of potential futures. ScenarioMIP expands upon the CMIP6 core simulations and multiple scenarios are available for modellers to use to generate simulations (O'Neill et al., 2016). We include the scenarios: SSP1-1.9, SSP1-2.6, SSP2-4.5, SSP3-7.0 and SSP5-8.5 (O'Neill et al., 2016; Riahi et al., 2017). Scenario names in CMIP6 are comprised of a general future pathway (SSP1-SSP5) followed by an estimate of the radiative forcing at the year 2100 in units of Wm^{-2}. These scenarios cover a wide range of possible futures, including sustainable development in the SSP1-1.9 and SSP1-2.6 scenarios. The intermediate emissions scenario or "middle of the road" pathway in SSP2-4.5 extrapolates historic and current global development into the future with a medium radiative forcing by the end of the century. The regional rivalry scenario, SSP3-7.0, revives nationalism and regional conflicts, pushing global issues into the background and resulting in higher emissions. Then finally, the enhanced fossil fuel development in SSP5-8.5 is a scenario with the highest feasible fossil fuel deployment and atmospheric CO_2 concentration (Riahi et al., 2017).

1.2 Climate Sensitivity

Given the same rise in atmospheric CO_2 concentration, each ESM will warm by a different amount due to the significant structural and parametric differences between models. The Equilibrium Climate Sensitivity (ECS) is a measure of this sensitivity to CO_2. The ECS is given in °Celsius and represents the long-term near-surface air temperature rise that is expected to result from a doubling of the atmospheric CO_2 concentration once the model has reached equilibrium. In effect, the ECS is an indicator for how much warming occurs in a model with a doubling of CO_2. The most recent 5-95% assessed natural ECS range was between 2 °C and 5 °C, the likely ECS range was 2.5 - 4 °C, and the most likely value was 3 °C (Arias et al., 2021, TS6).

The wide spread of ECS values in climate models is one of the causes of uncertainty for the timing of when forecasts reach certain warming levels. The "allowable emissions" that keep global temperature rise within policy targets are equally impacted (United Nations Treaty Collection, 2015). This has been exacerbated in the latest round of CMIP, as the CMIP6 generation

of ESMs has a broader range of sensitivities than previous generations. Several CMIP6 models have a stronger response to atmospheric carbon than any CMIP5 model, and many sit above the likely ECS range (Arias et al., 2021, TS6.).

1.3 Global Warming Levels

Climate change policy can often focus on the climate at specific target years, like 2050 or 2100 (United Nations Treaty Collection, 2015; IPCC, 2021a). However, due to the wide range of ECS values in ESMs, this can mean that ensembles at the year 2100 are composed of a set of models with significantly different behaviours. This wide range in the temperatures and warming rates at a given point in time has knock-on effects on feedbacks and may inhibit the realism and representivity of the ensemble multi-model mean (Hausfather et al., 2022; Swaminathan et al., 2022). Instead of specific target years, we can alternatively focus on model behaviour at specific Global Warming Levels (GWL), such as 2 °C, 3 °C or 4 °C of warming relative to the pre-industrial period. By investigating the system's behaviour at specific warming levels instead of target years, we can account for the impact of climate sensitivity and make policy relevant assessments while still exploiting the full ensemble of CMIP6 models. This allows us to maintain model democracy, even in a so-called "hot model" ensemble.

The 2, 3 and 4 °C GWLs were chosen because the 2 °C GWL is a key target set in the 2015 Paris Agreement (United Nations Treaty Collection, 2015) and thought to be a threshold for potentially dangerous climate change. The 3 °C GWL is the warming level that current nationally determined emission policies will realise for the year 2100 assuming a median climate sensitivity (United Nations Environment Programme, 2019). Finally, the 4 °C GWL is a low likelihood but high impact outcome if climate sensitivity is higher than median values or emission reductions and climate policy break down.

This is the first work that presents the carbon allocation using this GWL framework. Previous analyses project carbon allocation at an arbitrary point in time using the mean of a set of models with widely different warming rates and sensitivities (IPCC, 2021a; Canadell et al., 2021). When compared against projections at specific points in time, our results are less influenced by the overall sensitivity of the ensemble and may be more relevant to policymakers.

2 Methods

2.1 Carbon allocation calculation

We calculate the carbon allocation for the land, ocean and atmospheric reservoirs separately. On the land surface, the land carbon sink, S_{Land}, is derived from the global total net biome production (NBP) and the global total land use emissions (LUE). As NBP is defined as the difference between land sink and emissions from land use ($NBP = S_{Land} - LUE$), then:

$$S_{Land} = NBP + LUE \tag{1}$$

The NBP is an prognostic variable calculated by the models and it is defined as positive for fluxes into the land carbon store in CMIP6 (Jones et al., 2016). We calculated the global total net biome production as the cumulative sum over the entire global land surface of the NBP multiplied by the cell surface area. From CMIP6 simulations, it is not possible to directly isolate the LUE and so these are taken from land use scenarios common across all models and all ensemble members following Liddicoat

et al. (2021). As described in Pongratz et al. (2014) and Liddicoat et al. (2021), a more accurate method of determining the LUE is to calculate the difference in net biosphere production between a pair of simulations, one with land use changing over time, and the other with fixed land use. However, these simulation pairs exist only for a limited subset of models and scenarios. CMIP6 experiments express the LUE in units positive into the atmosphere, which is the opposite direction of the carbon flux in NBP.

The ocean component of the carbon allocation, S_{Ocean}, is the total global sum of the air sea flux of CO_2. We calculated this as the sum of the air-sea flux of CO_2 multiplied by the ocean area of each cell, expressed as a cumulative sum of the annual totals.

In the atmosphere, the global mean CO_2 concentration is provided in the scenario forcing from ScenarioMIP in units of parts per million (ppm). The total mass of the carbon in atmospheric CO_2, C_{Atmos} is calculated by multiplying the change in concentration relative to the 1850 value in ppm by a constant factor. This conversion factor is 1 ppm of CO_2 is equivalent to 2.13 PgC (Myers, 1983). No matter how much carbon the land and ocean components absorb from the atmosphere, the atmospheric concentration of CO_2 will always strictly follow the prescribed atmospheric CO_2 concentrations of the forcing scenario. This means that anthropogenic emissions can be estimated for each model (Jones et al., 2013). The total anthropogenic carbon, C_{Total}, is the sum of the total carbon in the atmospheric CO_2 and the cumulative global total CO_2 flux into the sea and the true land sink.

$$C_{Total} = C_{Atmos} + S_{Ocean} + S_{Land} \tag{2}$$

2.2 Included Models

This analysis used all CMIP6 ESMs for which the following three variables were available as monthly averages over the time period 1850-2100: the near-surface atmospheric temperature (tas), the net biome productivity (nbp) and the air to sea flux of CO_2 ($fgco2$). We limited each model to only the first ten ensemble members for each scenario, and required at least one historical and future scenario pair for each ensemble member. The grid cell area was also required for the ocean ($areacello$), and for land and atmosphere ($areacella$) grids. We excluded the entire ensemble member if any variables were absent, the time series was incomplete, or the data could not be made compliant with CMIP6 standards.

In CMIP6, modelling centres may contribute more than one ensemble member for each scenario to the Earth System Grid Federation (ESGF). For instance, the UKESM1 model produced 19 different variants for the historical experiment, each using slightly different initial conditions drawn from the pre-industrial control (piControl) simulation (Sellar et al., 2020). This generates an ensemble of variants which samples a wide range of the unforced variability simulated by the model. By spanning the range of internal variability simulated by the model, the mean of a single model ensemble can give a more robust estimate of the forced climate change. Each modelling centre may choose which scenarios they simulate and how many ensemble members are generated for each scenario. This means that there is wide variation in the number of ensemble members between models. To balance models with large ensembles against models with small ensembles, we used a “one model - one vote” weighting scheme. This ensured that each model was given equal weight in the final multi-model mean. In practice, each

ensemble member of a given model was weighted inverse proportionally to the number of ensemble members that the model contributed. No effort was made to weigh the results regarding the model quality or historical performance.

Table 1 lists the contributing models, the number of ensemble members for each scenario, and each model's equilibrium climate sensitivity (ECS). The ECS plays a first order role in how rapidly a given model reaches a given GWL for a given CO_2 pathway. For most models, we took the ECS value from Zelinka et al. (2020). For the models whose ECS was not included in Zelinka et al. (2020), we use the following ECS values: ACCESS-ESM1-5 from Ziehn et al. (2020), CMCC-ESM2 from Lovato et al. (2022b), EC-Earth3-CC from Hausfather et al. (2022), GFDL-ESM4 from Dunne et al. (2020), and MPI-ESM1-2-LR from Mauritsen et al. (2019). No ECS value was available for the CanESM5-CanOE model as it did not provide the abrupt $4xCO_2$ experiment required to calculate ECS using the Gregory method (Gregory et al., 2004; Christian et al., 2022). However, it only differs from CanESM5 by the addition of a marine biogeochemistry component model (Swart et al., 2019; Christian et al., 2022). We follow the method used elsewhere (Hausfather et al., 2022; Scafetta, 2022), and substitute CanESM5's ECS value for CanESM5-CanOE. Other ECS datasets also exist, see for instance: Flynn and Mauritsen (2020); Meehl et al. (2020); Weijer et al. (2020); Hausfather et al. (2022), and only have small differences in their values. All ECS values included here use the Gregory et al. (2004) method, however, the value of ECS for any given model is sensitive to the method that was used to derive it. See for instance tab. 4 of Boucher et al. (2020), where ECS for the same model varies by more than a degree depending on the methodology.

This table also shows the ensemble mean ECS of the contributing models for each scenario in the last row. The weighted ECS is only weighted by the presence or absence of models, not the number of contributing ensemble members, reflecting the "one-model one-vote" weighting scheme described above. The spread of weighted ECS values between scenarios is small, ranging from 3.96 for SSP1-1.9 to 4.17 for SSP5-8.5. Five out of six of these ensemble means sit above the likely ECS range of 2.5°C - 4 °C, and four of the individual models are outside the 5-95% confidence band, 2 °C and 5°C (Sherwood et al., 2020; Arias et al., 2021).

As in other CMIP ensemble studies, we attempt to maximise the number of models in this work (Flynn and Mauritsen, 2020; Meehl et al., 2020; Weijer et al., 2020; Hausfather et al., 2022), so we allow all available candidates, even pairs of sibling models: there are two CESM2 models and two CanESM5 models in the ensemble. CESM2-WACCM6 is configured identically to CESM2, except that it has expanded aerosol chemistry and uses 70 vertical levels and its model top is at 4.5×10^{-6} hPa (approximately 130 km), instead of CESM2's 32 vertical levels and a model top at 2.26 hPa (approximately 40 km) (Danabasoglu et al., 2020). The CanESM5-CanOE model differs from CanESM5 by the addition of a more complex marine biogeochemistry component (Christian et al., 2022).

In addition to sibling models, the same individual component models are used by several modelling centres. For instance, the NEMO ocean circulation model forms the marine circulation component model of six of the earth system models used here (Lovato et al., 2022a). While the ESMs use differing versions of NEMO with different configurations and settings, these models can not be treated as statistically independent. However, it is beyond the scope of this work to develop or apply a method to weight models such that the multi-model mean is statistically robust, for instance in Brunner et al. (2020).

Table 1. A list of the models, the number of contributing ensemble members for each scenario, the model ECS, and the weighted mean ECS of the contributing models. The weighted ECS row shows how the model occupancy affects the mean ECS of the ensemble for each scenario. The presence or absence of models impacts the weighted ECS, but not the number of contributing ensemble members.

Model	Historical	SSP1-1.9	SSP1-2.6	SSP2-4.5	SSP3-7.0	SSP5-8.5	ECS
ACCESS-ESM1-5	3		2	3	2	1	3.87
CESM2	3		3	3	3	3	5.15
CESM2-WACCM	3		1	3	1	3	4.68
CMCC-ESM2	1			1			3.57
CanESM5	10	10	10	10	10	10	5.64
CanESM5-CanOE	2		2	2	2		5.64
EC-Earth3-CC	8			8		1	4.23
GFDL-ESM4	1	1	1	1	1	1	2.7
IPSL-CM6A-LR	12	5	3	6	10	5	4.56
MIROC-ES2L	5	5	5	5	5	5	2.66
MPI-ESM1-2-LR	5	5	5	5	5	5	2.83
NorESM2-LM	2		1	2	1		2.56
UKESM1-0-LL	10	5	10	10	10	5	5.36
Total number of Ensembles	65	31	43	59	50	39	
Total number of Models	13	6	11	13	11	10	
Weighted ECS	4.11	3.96	4.15	4.11	4.15	4.17	

2.3 Global warming level calculation

We calculated the global warming level following the methods of Swaminathan et al. (2022). The global mean atmospheric surface temperature is calculated for each model, scenario and ensemble member. The anomaly is the difference from the mean of the period 1850-1900 from the relevant historical ensemble member. This temperature time series is then smoothed by taking the mean of a window with a width of 21 years, i.e. 10 years either side of the central year. The first year that the smoothed global mean surface temperature anomaly exceeds the global warming level is the GWL exceedance year (see Fig. 1 of Swaminathan et al. (2022)). Note that due to the 21 year window, the last possible GWL threshold year is 2090.

We calculate the multi-model mean for each of the variables using the "one model - one vote" scheme described above. We also determine the multi-model mean GWLs and their timings from the multi-model mean temperature, instead of taking the weighted mean of the individual ensemble members GWLs timings. This method ensures that the multi-model mean is more representative of the overall ensemble, instead of biased towards only those models that reach the GWL.

We used the ESMValTool toolkit to perform the analysis. ESMValTool is a software toolkit that was built to facilitate the evaluation and inter-comparison of CMIP datasets by providing a set of modular and flexible tools (Righi et al., 2020). These

tools include quick ways to standardise, slice, re-grid, and apply statistical operators to datasets. In our case, we used the annual_statistics preprocessor to calculate the annual mean, the mask_landsea preprocessor to mask the land or ocean areas, and the area_statistics preprocessor to calculate the area weighted global mean. ESMValTool is hosted on GitHub and all the code we used here is available as described in the data availability section.

3 Results

3.1 Multi-model mean carbon allocation

The total multi-model mean carbon allocation for each scenario at the year 2100 and for each of the three warming levels is shown in fig. 2. The left side shows the percentage allocation, and the right side shows the totals in PgC. In the top panes showing the carbon allocation at the year 2100, the higher emission scenarios have greater total carbon allocations with more of that carbon is allocated to the atmosphere, relative to the lower emission scenarios. At the year 2100, more carbon is allocation to the ocean than the land in SSP5-8.5, SSP3-7.0 and SSP2-4.5, while more carbon is allocation to the land than the ocean in SSP1-2.6, SSP1-1.9. This reproduces the results discussed earlier from (IPCC, 2021b, fig. SPM7).

The lower three rows of this figure show the carbon allocation at each GWL. In all cases, the variability between scenarios within a single GWL is significantly less that the variability between scenarios at the year 2100 in the top pane. However, the variability within the same GWL is still significant in absolute terms. For instance, the multi-model mean 2 °C GWL ranges from 909 PgC in SSP2-4.5 to 972 PgC in SSP3-7.0 (a range of 63 PgC). At the 3 °C GWL, the range is 56 PgC and at 4 °C GWL, the range is 15 PgC. When compared against the annual total emissions estimate, 9.4 ± 0.5 PgC yr^{-1} (Le Quéré et al., 2018), these differences between scenarios represent several years worth of the global total anthropogenic emissions.

In the land surface, the multi-model mean 2 °C GWL has a range of 46 PgC, 35 PgC at the 3 °C GWL, and at 4 °C GWL, the range is 52 PgC between scenarios. The recent annual terrestrial carbon sink was 3.2 ± 0.8 PgC yr^{-1} (Le Quéré et al., 2018), so the difference between scenarios is equivalent to at least a decade worth of current carbon absorption by the land surface.

In the ocean, the 2 °C GWL carbon allocation has a range of 28 PgC, the 3 °C GWL has a range of 34 PgC, and at 4 °C GWL has a range of 21 PgC between scenarios. This reflects the previous result that the carbon allocation to the land surface is more variable than the ocean, as the land values have a wider range. The recent annual ocean carbon sink was 2.4 ± 0.5 PgC yr^{-1} (Le Quéré et al., 2018). Similarly to the land case described above, the difference between scenarios is equivalent to approximately a decade worth of current ocean carbon absorption.

In the left hand side of fig.2, the higher CO_2 concentration scenarios have a larger atmospheric fraction than lower CO_2 concentration scenarios at the same GWL. For instance, the atmospheric fraction is 46% in SSP5-8.5 and 42% SSP1-2.6 at the 2 °C GWL, and the atmospheric fraction is 51.2% in SSP5-8.5 and 47.4% SSP2-4.5 at the 3 °C GWL.

Figure 2 only shows the multi-model means, not single models. This means that multi-model means that do not reach the GWL are not included in this figure. Table 1 shows that there are six models contributing to the SSP1-1.9 scenario in this analysis, yet the multi-model mean does not reach the 2 °C GWL here. Similarly, there are 11 SSP1-2.6 models, but the multi-

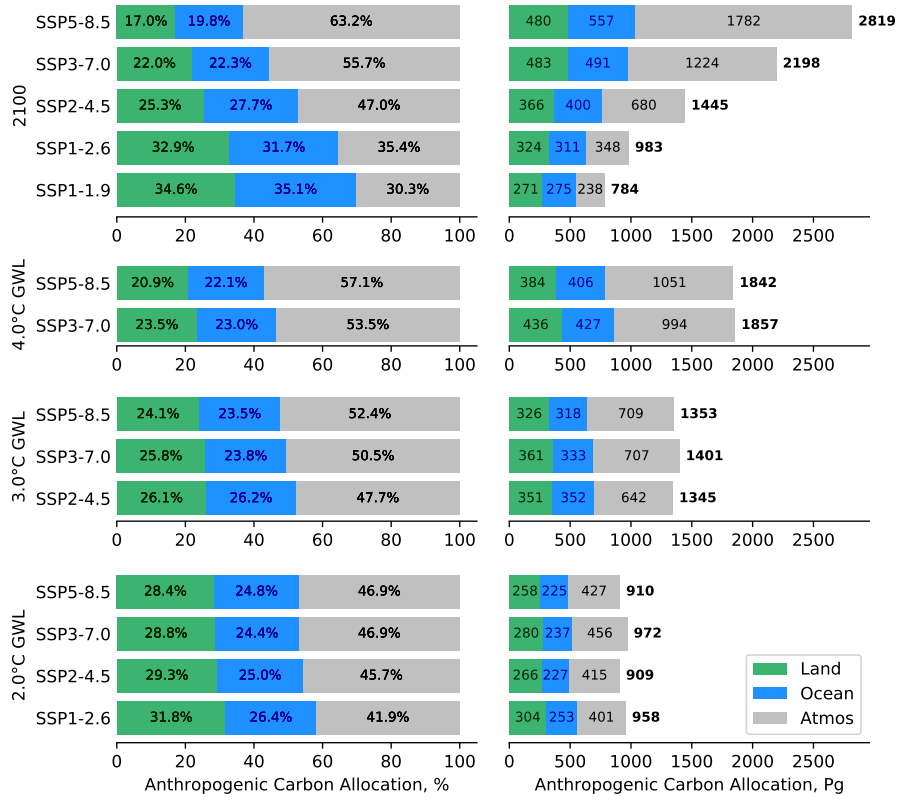

Figure 2. Carbon allocation for the multi-model mean for each scenario for the year 2100 and the three GWLs. The green, blue and grey areas represent the land, ocean and atmospheric carbon allocations. On the left hand side, the x-axis shows the carbon allocation as a percentage, and the right hand side shows the cumulative total. The total values are shown in bold to the right of the bars. Note that these values are rounded to the nearest integer, so the three values may not add exactly to the total.

model mean does not reach the 3 °C GWLs before the year 2100, nor does the mean of the 13 SSP2-4.5 models reach the 4 °C of warming.

3.2 Carbon allocation time series

The CMIP6 multi-model mean carbon allocation time series is shown in fig. 3. This figure includes a pair of panes for each scenario. For each pair, the top pane is the cumulative carbon in PgC and the bottom pane shows the percentage. The sum of the three sinks estimates the total anthropogenic emissions. The top left pair shows the development over the historical period and the other five pairs show the future scenarios. We include all data cumulatively from the year 1850, and all the cumulative carbon panes share the same y-axis range. The timing of each of the multi-model mean GWLs are marked as vertical lines.

In the historical pane of fig. 3, the fractional atmospheric carbon starts to grow in the second half of the 20^{th} century, as the land fraction declines and the ocean fraction increases. However, all three reservoirs increase in absolute terms over the entire

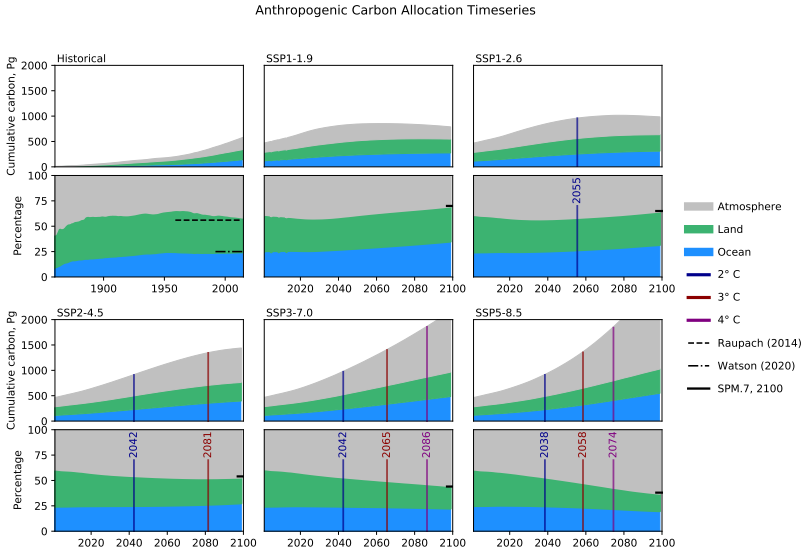

Figure 3. Multi-model mean carbon allocation time series for the historical period and each scenario. The top pane of each pair shows the total allocation in PgC, and the bottom pane shows the allocation as a percentage. The historical pane includes the historical observations from Raupach et al. (2014) & Watson et al. (2020), and the length of the lines represent the time over which the data was collected for these two observational datasets. The future pane shows the atmospheric fraction projection for 2100 from IPCC (2021b). The grey area is the cumulative anthropogenic carbon in the atmosphere, and the blue and green represent the fraction in the ocean and in the land, respectively. The SPM7 lines at the year 2100 indicate the atmospheric fraction projections from the IPCC AR6 WG1 summary for policymakers figure 7, IPCC (2021b).

historical period. By the end of the historical period, the land and ocean match the observational records of Raupach et al. (2014) and Watson et al. (2020) reasonably well, shown as dashed horizontal lines. In future scenarios, the global warming level threshold year occurs sooner in higher concentration scenarios than in lower concentrations scenarios. In all scenarios, the total anthropogenic carbon rises until at least the year 2050. In the two SSP1 scenarios, the total carbon starts to fall after this point, while it continues to grow in the other projections.

The fraction of carbon that is absorbed by the combined land and ocean reservoirs rises in the two SSP1 scenarios, remains approximately constant in SSP2-4.5 after 2050, and declines in the SSP3-7.0 and SSP5-8.5 scenarios. The time series at the year 2100 closely match the IPCC atmospheric fraction projections for the year 2100 (IPCC, 2021b, fig. SPM7), shown in fig. 3 as a horizontal line at the end of the period. This corroboration of existing results allows an increased confidence that our methodology is correct.

3.3 Multi-model ensemble carbon allocation

Figure 4 shows the carbon allocation at each GWL as a percentage and in terms of the total carbon for each model. For each scenario and each GWL, the models are ordered by their ECS as shown in tab. 1. The lower ECS models are at the top and higher ECS models on the bottom of each section. The lower sensitivity models take longer to reach the same warming level and have more total emissions than the higher sensitivity models. This results in the saw-tooth pattern on the right of this figure. However, this saw-tooth pattern does not appear on the left side of the figure, as the ratios of carbon allocation between land, ocean and atmosphere at a given GWL are not dependent on ECS.

There is a significant variability between individual models in the total carbon between scenarios at each GWL. For instance, the total carbon at 2 °C ranges from 615 PgC (CanESM5-CanOE, SSP3-7.0) to 1521 PgC (NorESM2-LM at SSP3-7.0). This range of behaviours between models is very large and the difference between these two extremes is equivalent to a century's worth of current global emissions (ie 100 years of 9.4 ± 0.5 PgC yr^{-1} Le Quéré et al. (2018)).

Proportionally large ranges can also be seen in the land, ocean and atmospheric carbon sinks in fig. 4. For instance, at 2 ° C warming, the land may have absorbed as little as 164 PgC (EC-Earth3-CC SSP2-4.5), or as much as 432 PgC (MIROC-ES2L, SSP3-7.0). Similarly, at at 2 ° C warming, the ocean may have absorbed as little as 137 PgC (CanESM5-CanOE SSP3-7.0) or as much as 401 PgC (NorESM2-LM SSP2-4.5). These ranges are equivalent to several decades worth of current global emissions, or approximately a century of the current annual rates of land or ocean carbon absorption.

The left side of this figure shows several key results related to how carbon is allocated as a percentage of the total between models. Firstly, at a given GWL, higher emission scenarios have a higher atmospheric fraction. In effect, the SSP5-8.5 scenarios have a higher atmospheric fraction than SSP1-1.9 and SSP1-2.6 scenarios, even at the same GWL. Similarly, higher emission scenarios have a smaller land fraction, while the ocean fraction is similar across scenarios at the same GWL. Secondly, warmer GWLs have a larger atmospheric fraction than cooler GWLs. Thirdly warmer GWLs have a smaller land fraction than cooler GWLs. Finally, the ocean fraction is relatively consistent between GWLs and scenarios.

3.4 Carbon allocation and ECS

The data from fig. 4 is re-framed in fig 5 as a series of scatter plots. In this figure, each row represents a different scenario, and each column is a different dataset. These datasets are: the GWL threshold year, the total carbon allocated, the carbon allocation for each domain and the fractional carbon allocation to each domain. The y-axis shows the model's ECS, and each point is a different GWL, where the squares are 2 °C GWL, the circles are 3 °C GWL, and the triangles are 4 °C GWL. The multi-model mean is shown with the same shape but hollow. In all cases, the darkest colours are the 2 °C GWL, the middle colour are the 3 °C GWL, and the lightest colours are the 4 °C GWL. For each group of data, the line of best fit is shown and the absolute value of the fitting error (Err) of the slope (M) over the slope is shown in the legend, as Err/M. The fitting error, Err, here is the standard error of the estimated gradient under the assumption of residual normality. This value indicates whether the slope crosses the origin within the 95% confidence limit. If the uncertainty on the slope is greater than the slope itself (and Err/M

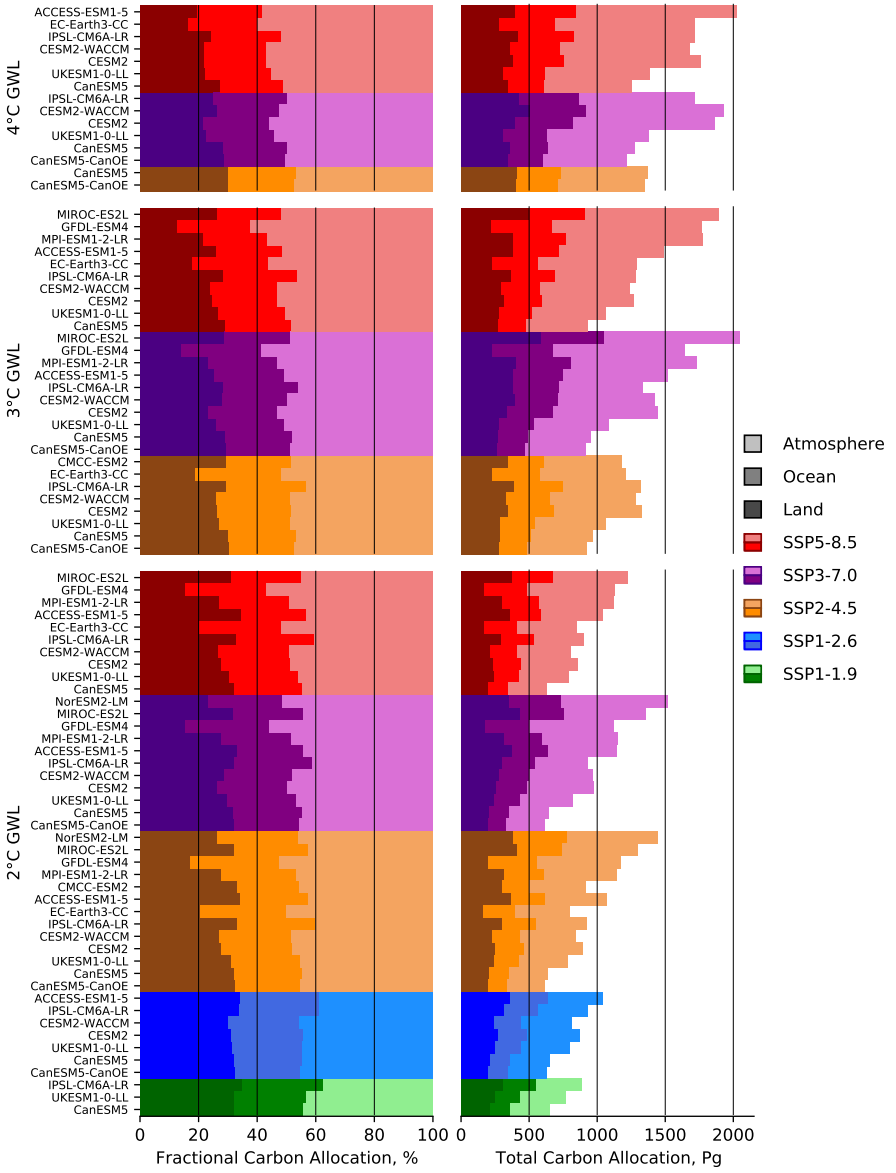

Figure 4. Global total carbon allocation for each level of warming for individual models. The left side shows the allocation as a percentage and the right side shows the total value in PgC. Each colour palette represents a different scenario, with SSP1-1.9 in greens, SSP1-2.6 in blues, SSP2-4.5 in oranges, SSP3-7.0 in purples and SSP5-8.5 in reds. The darkest shade denotes the land, the middle shade is the ocean and the lightest shade is the atmosphere. Within a given GWL and scenario, the models are ordered by their ECS, with less sensitive models at the top and more sensitive models at the bottom.

exceeds unity), then we can assume that the fit is not statistically significant. All groups with three models or fewer that reach the GWL were excluded as this is not enough data points to draw meaningful conclusions.

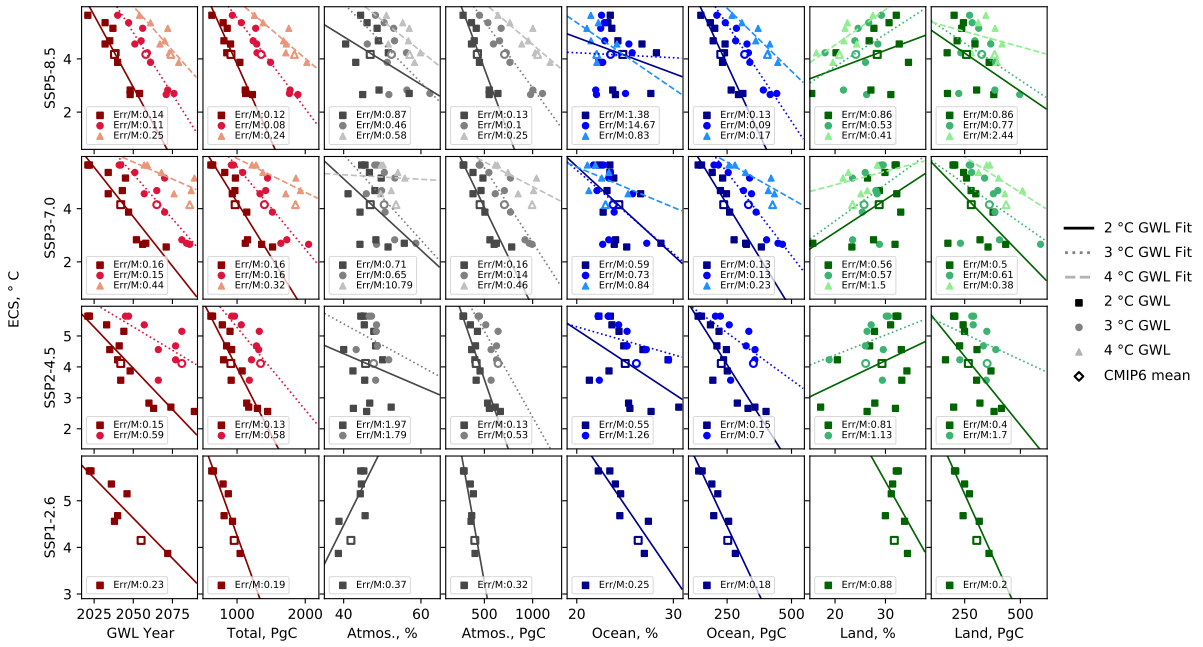

Figure 5. GWL carbon allocation scatter plot matrix for each. each row represents a different scenario, and each column is a different data field, including the GWL year, the total carbon allocated, the carbon allocation for each domain and the fractional carbon allocation to each domain. The y-axis is the model's ECS, and each point is a different GWL, where the squares are the 2° GWL, the circles are the 3° GWL, and the triangles are the 4° GWL. The multi-model mean is shown with the same shape but hollow. In all cases, the darkest colours is the 2° GWL, the middle colour are the 3° GWL, and the lightest colours are the 4° GWL. For each group of data, the line of best fit is shown and the absolute value of the fitting error of the slope over the slope is shown in the legend.

The goal of this figure is to highlight in broad strokes the ways that ECS interacts with carbon allocation in these models. In most of the fits, the data and the ECS are inversely correlated such that lower ECS models have higher values. This appears to be true for GWL year, total carbon and the individual total carbon fields in the atmosphere, ocean and land. The GWL threshold year and the total carbon allocations both have all absolute Err/M values lower than unity and as such are both related to ECS. In both the ocean and the atmosphere's total carbon, the absolute value of Err/M is always smaller than one. This means that the total carbon in both the ocean and the atmosphere are linked to ECS with 95% confidence. However, this is not the case for the ocean or the atmosphere's carbon allocation as a percentage and in many cases absolute Err/M is greater than unity. This means that we can not say that the fraction of carbon allocated to the ocean or to the atmosphere is related to the ECS with 95% confidence. Similarly, this absolute Err/M ratio is not consistently below unity for the land ensembles at all GWLs. This implies that the total or percentage land carbon allocation is likely to be not correlated with ECS.

By including the multi-model mean as a hollow shape in fig. 5, we can estimate the representivity of the group of models that reach the GWL relative to the entire ensemble which may include several models which do not reach the GWL. If the mean sits at the lower end of the ECS range, then it is likely that several models did not reach the GWL.

4 Discussion

We have shown an analysis of the carbon allocation in the Earth System for an ensemble of CMIP6 simulations at three warming levels. By using the GWL method instead of focusing on a specific target year, we can provide estimates of the behaviour of the carbon cycle that may be more useful and relevant to policy-makers. In fig. 2, the difference between a focus on a specific year and the GWL method can clearly be seen by comparing the top pane against the other three panes. At the year 2100, there are large differences between the five scenarios total carbon, the allocation between the three reservoirs and the fractional distribution. In the lower three panes, the differences between scenarios is much smaller. However, these small differences are still significant in absolute terms, where several years worth global CO_2 emissions separate the scenarios at each GWL. The pathway to a given GWL is scenario dependent in two main ways. Firstly, the rate of anthropogenic CO_2 emissions has a non-negligible impact on the atmospheric fraction because the ocean and land surface can not quickly absorb the additional carbon load. A higher rate of emission leads to a slightly greater transient warming, because fractionally more of the emitted CO_2 is still in the atmosphere. Secondly, CO_2 is the primary but not the only driver of warming. Differences between the non-CO_2 forcings play a role in the realised warming at a given point in time in these scenarios. In addition, while the composition of each scenario ensemble results in a relatively uniform set of values of the mean ECS in tab. 1, the mean ECS does vary by up to 0.21 °C between scenarios. This could also account for some of the differences seen between multi-model means in fig. 2. Furthermore, the SSP1-1.9 ensemble has the lowest mean ECS and the SSP5-8.5 ensemble has the highest mean ECS, which may exaggerate the differences between them.

The GWL methodology allows a focused analysis on the small and subtle differences between scenarios seen elsewhere. For instance in Canadell et al. (2021), fig. 5.31 shows the cumulative carbon emissions against global mean temperature change for several projections. In that figure, all five projections show a strong correlation between CO_2 emissions and warming. In addition, all projections overlap at the same cumulative CO_2 emissions. Due to results like these, it is widely thought that there are not significant differences in the carbon behaviour of these scenarios for the same cumulative CO_2. Using the GWL method, we have placed these results under the microscope and demonstrated that for carbon allocation, small differences exist between scenarios and that the pathway to a GWL matters. However, these differences in carbon allocation may only be visible under the zoomed-in focus of a GWL analysis. The differences between scenarios are consistent with previous studies and are likely due to differences in non-CO_2 forcing. It is beyond the scope of this work to quantity the non-CO_2 effect.

On the left side of fig. 2, the fraction of carbon that remains in the atmosphere is linked with the choice of scenario. The higher emission scenarios have higher atmospheric fractions (AF) at the same warming level. The mechanism here is most likely to be that scenarios with higher carbon concentrations simply reach the global warming levels sooner, and have proportionally less carbon allocated to the ocean and land surface at that time. The ocean and the land hasn't had time to catch up with the emissions or the warming associated with that carbon dioxide concentration. This implies that the carbon allocation between the three major sinks is likely impacted by the rate of warming at the GWL and there may be some delay between CO_2 emissions and the equilibrium CO_2 atmospheric fraction, as the excess CO_2 is slowly absorbed by the terrestrial and oceanic sinks.

In the land surface at the 4° C GWL, the multi-model mean land vegetation carbon increases by 384 and 436 PgC relative to 1850 in SSP5-8.5 and SSP3-7.0 respectively, as shown in fig. 2. In Friend et al. (2014), the range relative to the years 1971-1999 was 52–477 PgC with a mean of 224 PgC, and was attributed mainly due to CO_2 fertilisation of photosynthesis. While our CMIP6 multi-model mean is compatible with Friend et al. (2014)'s CMIP5 result, we do not see any individual model with only 52 PgC carbon allocated to the land at the 4° C GWL in fig 4. This absence is more likely to be attributed to the difference in the anomaly period (1850 vs 1971), rather than due to the significant changes between CMIP5 and CMIP6 land surface models. The model that contributed 52 PgC in Friend et al. (2014)'s CMIP5 analysis, VISIT, is part of the MIROC-ES2L ESM in CMIP6 (Hajima et al., 2020). However, MIROC-ES2L did not reach the 4° C GWL in any scenario presented here. In all aspects of this analysis, the land carbon allocation has a much wider range of variability than the ocean. This reflects the significant challenge and uncertainty inherent in modelling the land surface carbon cycle (Friend et al., 2014; Jiang et al., 2019).

When comparing the same model at the same GWL between scenarios, the differences between scenarios becomes even more apparent, as shown in fig. 4. This is especially true for low ECS models. For instance, the minimum and maximum carbon allocation in the MIROC-ES2L at 2 °C GWL is 1225 PgC in SSP5-8.5 and 1361 PgC in SSP3-7.0. The difference between these two projections of the same model with the same warming level is 136 PgC. For the decade 2008–2017, the mean annual emissions were 9.4 ± 0.5 PgC yr^{-1}, so this difference alone is equivalent to approximately 14 years of our entire current total global emissions.

In fig. 4, when comparing individual models between different GWLs, the highest total carbon allocation at the 2 °C GWL is 1521 PgC (NorESM2-LM SSP3-7.0). This is more total carbon than several models emitted at higher GWLs: the lowest carbon emitted at 4 °C GWL was 1220 PgC for CanESM5-CanOE in the SSP3-7.0 scenario. In addition, both CanESM5 models and the UKESM1 model reached 4 °C of warming in three different scenarios with less atmospheric carbon than NorESM2-LM had when it reached the 2 °C GWL. This highlights the significant role that ECS plays in the uncertainty of warming projections. A model's sensitivity to CO_2 concentration significantly impacts its projection of the total carbon allocation at global warming levels, as well as the absolute values of the individual carbon sinks in the ocean and land.

The ocean maintains similar allocation percentages across the GWLs, but in fig. 3 there is a small decline in ocean carbon allocation percentage at the highest CO_2 concentration scenarios towards the end of the 21^{st} century. This is likely because much of the ocean is forecast to become increasingly stratified in the coming century, which would reduce downwards mixing of CO_2 (Li et al., 2020; Muilwijk et al., 2023). This reduction in downward mixing combined by the decline in solubility with rising sea surface temperature, causes the overall absorption rate is of CO_2 into the ocean to be reduced. The increase in stratification is caused by warmer surface layers, combined with gradual decline in overturning rates and overall circulation (Thibodeau et al., 2018; Li et al., 2020; Caesar et al., 2021; Sallée et al., 2021). Ocean acidification may also be playing a role reducing the chemical transition of dissolved CO_2 and thus also slowing uptake (Zeebe, 2012). In combination, these effects act to reduce the rate absorbed CO_2 is removed from the surface layer.

While the ocean fraction is more or less consistent throughout the SSP2-4.5, SSP3-7.0 and SSP5-8.5 scenarios at the GWLs, the land fraction declines over the coming century in fig. 3, from 35% at the end of the historical period to 25.3% in SSP2-4.5,

22% in SSP3-7.0 and 17% in SSP5-8.5 at the year 2100. The land fraction is forecast to decline over the coming century in the higher CO_2 concentration scenarios, although the total land carbon allocation increases. There are several possible explanations for this slowdown of uptake. The soil respiration could increase due to warming more than the carbon uptake increase due to photosynthetic uptake (Nyberg and Hovenden, 2020). Alternatively the nitrogen limitation could progressively limit photosynthetic uptake (Ågren et al., 2012). The changing climate may impact vegetation growth and photosynthetic uptake via droughts and warming, which moves plants outside the most efficient temperatures for photosynthesis. It is not clear from this work which factors have the largest impact.

The differences in carbon allocations seen here have consequences in the real world. Global warming and higher CO_2 increases the regional and temporal variability of precipitation (Tebaldi et al., 2021). There is also the direct effect of increasing atmospheric CO_2 on radiative cooling rates. This impacts the vertical thermal structure of the atmosphere and thus tropical overturning circulations and regional precipitation. This direct effect of atmospheric CO_2 is independent of the level of warming (Bony et al., 2013). This means that models or scenarios that have a greater atmospheric fraction of CO_2 at a given GWL will be more prone to this regional response to changed atmospheric radiative cooling, stability and circulation change, than models or scenarios with a smaller CO_2 fraction in the atmosphere.

Land ecosystems become progressively less efficient at absorbing carbon as levels of CO_2 concentrations atmosphere increase (Wang et al., 2020). In the ocean, higher CO_2 causes enhanced ocean acidification, which has a range of effects but has been shown to decrease survival, calcification, growth, development and abundance over a broad range of marine organisms (Kroeker et al., 2013).

4.1 Survivor bias

Not all scenarios are expected to reach these warming thresholds before the year 2100. While it is highly likely that all SSP5-8.5 will reach 2 °C of warming, it is unlikely that any SSP1-1.9 experiments will reach 4 °C of warming. This is why the 4 °C GWL pane of fig. 2 only includes two multi-model means, while the 2 °C GWL pane includes four. On the other hand, in certain combinations of scenario and GWL, it is possible that only some models reach the threshold. For instance, three of the six SSP1-1.9 models reach the 2 °C GWL. As described above, the method that we used to populate fig. 2 took the multi-model mean first with all models contributing equally, then used that ensemble mean to calculate the GWL threshold years. An alternative method could first calculate the GWL threshold years for individual ensemble members, then take the mean of only those that reach the threshold. This alternative method would implicitly include survivor bias, causing the overall weighting and conclusions to be biased towards high ECS models.

The SSP1-1.9 scenario includes data from 6 models, yet only three models reach the 2 °C GWL, as can be seen by comparing tab. 1 and fig. 4. Similarly, the SSP2-4.5 scenario includes data from 13 models, yet only two models reach the 4 °C GWL. These missing models would most likely reach the thresholds at some point after the year 2100, if allowed to run for enough additional years with positive net CO_2 emissions.

4.2 Impact of ECS

The ensemble of CMIP6 models has a wide range of ECS values, and their sensitivity to carbon impacts several aspects of carbon allocation. The GWL threshold year and the total carbon are both inversely correlated with ECS. Similarly, the carbon in the atmosphere and allocated to the ocean are both inversely correlated with ECS. The ECS does not appear to be consistently correlated with the total land carbon allocation or the land carbon fraction at all scenarios and GWLs. The wider uncertainty and challenging nature of land surface carbon modelling is reflected in a broader range of behaviours in land carbon models in CMIP6.

The ECS impacts the GWL threshold year, but this range is also affected by the survivor bias described above. While we hesitate to draw conclusions from extrapolating the lines of best fit of fig. 5, the line of best fit for the 2 °C GWL threshold year for the SSP1-2.6 scenario crosses the year 2100 at a ECS equivalent to 3.1 °C. As the likely range of ECS values could be as low as 2.5 °C, this means that a non-trivial part of the ECS-phase space could be excluded by the ScenarioMIP limit of forecasting to the year 2100. Note that with the method we used to calculate the GWL year uses a smoothing window of 21 years, so the last possible GWL threshold year is 2090. While we could extend the analysis with some longer term simulations, very few models and scenarios are available beyond the year 2100. To address this issue, the next round of ScenarioMIP for CMIP7 could extend its standard cut off beyond the year 2100. This would reduce survivor bias at 2 °C GWL and allow the inclusion of models with a low but still feasible ECS of 2.5°C.

We have used the terms effective climate sensitivity and equilibrium climate sensitivity interchangeably. However, they do not measure the same thing. As an example, in Gjermundsen et al. (2021), they compared two Earth system models (NorESM2 and CESM2) that had the same atmospheric model but different ocean components. These two models were similar, but had very different ECS values: NorESM2's ECS is 2.56 °C and CESM2's ECS is 5.15 °C. In that work, they found that the greater heat storage at depth in NorESM2 delayed the Southern ocean surface warming and associated cloud responses, which in turned delayed global surface warming. This delay in the global surface warming was seen in the $4xCO_2$ simulations that are used to derive ECS. However, the Gregory method (Gregory et al., 2004) calculates the effective climate sensitivity with only 150 years of simulated climate while this effect appeared several centuries later. If both models were left to run long enough then the same cloud feedback eventually occurs in both models, the same amount of warming is realized, and the two models would have similar equilibrium climate sensitivities. In effect, the effective climate sensitivity that we've been using does not tell the entire story for the eventual realized warming from a given cumulative emission, because it is not fully compatible with the true equilibrium climate sensitivity. It may be possible to take this effect into account in future works, for instance, by replacing the surface atmospheric warming anomaly with some measure of the global volume-weighted mean ocean heat anomaly. However, the GWLs are defined in several international policy documents whereas the ocean heat content anomaly is less widely accepted outside earth system sciences.

4.3 Anomalous behaviour in SSP3-7.0

The SSP3-7.0 scenario often appears to be an outlier, for instance, in figs. 2 and 4, it does not conform to the pattern of the other scenarios. Also, in fig. 4, SSP3-7.0 is the scenario showing the widest range of carbon allocation behaviours at both the 2 °C and 3 °C GWLs. The SSP3-7.0 scenario has the highest methane concentration and air pollution precursor emissions forcing, even higher than those in SSP5-8.5 (Meinshausen et al., 2017, 2020). Methane is a strong greenhouse gas and has a warming effect, but pollution precursor emissions are linked to aerosols and cloud formation, which generally have a cooling effect (Twomey, 1977; Meinshausen et al., 2017). In CMIP6, methane warming can overwhelm, be overwhelmed by, or balance with aerosol cooling and the relative strengths of these effects depend strongly on the model parameterisation choices and their relative strengths in the scenario forcing. The relative strength of the warming methane emissions and the cooling aerosol precursors determines the impact on the warming rate and hence the GWL timing. While in other scenarios the methane and aerosol precursors scale approximately in proportion to the CO_2, in SSP3-7.0, they are significantly higher. Therefore, SSP3-7.0 scenarios may have a noticeably different warming response to CO_2 and its warming is not as tightly bound to the atmospheric CO_2 concentration after the year 2050 as in other scenarios. So while warming is still correlated to total cumulative emissions, SSP3 scenarios may reach the GWLs relatively earlier or later than other scenarios at the same CO_2 concentration. This effort could be investigated in detail if for instance the SSP3-8.5 or SSP5-7.0 scenarios were simulated.

In any case, the impact of different methane and aerosol precursor emissions on the climate response remains highly uncertain in CMIP6. The overall warming impact of methane is not further considered in this work as is it secondary to CO_2 warming, but it could be examined in future extensions.

4.4 Limitations and possible extensions

While the CMIP6 experiments start in 1850 from a pre-industrial control, clearly this is not the starting point for the anthropogenic impact on the land surface or the carbon cycle. Changes to the carbon cycle began much earlier and this has implications for ongoing carbon partitioning (Bronselaer et al., 2017; Le Quéré et al., 2018; Friedlingstein et al., 2022). For instance, between 1765 and 1850, atmospheric CO_2 rose by roughly 10 ppm, and accounting for this era resulted in a 4.5% change in ocean uptake in CMIP5 models (Bronselaer et al., 2017).

Similarly, the representation of dynamic vegetation, soil carbon and fire response is most likely under-sampled in this ensemble (Arora et al., 2020; Koch et al., 2021). Notably, CMIP6 models are not capturing present-day tropical forest carbon dynamics; the multi-model mean estimate of the pan-tropical carbon sink is half of the observational estimate (Koch et al., 2021). This uncertainty in the strength of carbon–concentration and carbon–climate feedbacks over land is well known (Cox et al., 2000; Friedlingstein et al., 2006; Arora et al., 2013).

The global ocean carbon inventory is also affected by the land-to-ocean carbon flux from river runoff and the carbon burial in ocean sediments, which is not represented in our ensemble (Arora et al., 2020). The flux of land carbon into the ocean via rivers is between 0.45 ± 0.18 PgC yr^{-1} and 0.78 ± 0.41 PgC yr^{-1} and is generally not considered in ESMs (Jacobson et al., 2007; Resplandy et al., 2018; Hauck et al., 2020). Including the riverine flux of particulate and dissolved organic carbon

would require models to represent both estuarine and shallow shelf processes. This would most likely require higher model resolutions and computational costs.

One of the limitations of the GWL methodology is that it focuses on the realized warming at a specific point in time. This is the transient warming, and it is unlikely that this warming includes the full effect of all cumulative CO_2 emissions. In effect, the CO_2 emissions have not yet played out to equilibrium, and there is likely to be a continued delay in their warming effect.

In this work, we used concentration driven scenarios instead of emission driven scenarios. Emission driven scenarios allow significantly more flexibility in the behaviour of the atmospheric carbon, in effect adding a third degree of freedom into the calculation. Although a limited set of emission driven runs exist, it was found that there are actually very few differences in simulated temperature or atmospheric CO_2 concentration between concentration driven and emission driven scenarios (Lee et al., 2021, Sec. 4.3.1.1). In any case, several key datasets required in the calculation of the land use emissions (LUE in eq. 1) were not available in the emission driven experiments at the time of writing.

In fig. 3, the multi-model mean of both SSP1 scenarios shows signs of recovery and carbon drawdown. In future versions of this work, it would be interesting to examine whether the carbon allocation behaves similarly on the way down as it did on the way up. More generally, extension simulations beyond 2100 would be valuable for studying how patterns of carbon allocation change as emissions decline past net zero.

In fig 5, we generated a fit to each dataset against the ECS. This fit is built on the assumption that these behaviours are linear and that the straight line fit is a reasonable approximation of their behaviour. However, as can be seen in this figure, this is not true in all cases. Several of the datasets have non-linear behaviours with regards to ECS. It may be possible to expand upon this work and generate more complex fits to these datasets to estimate the behaviour of these models within the likely ECS range of 2.5-4 °C.

While we made every effort to build a uniform ensemble, ScenarioMIP's flexible contributions means that we have a diversity in data occupancy between scenarios. The SSP5-8.5 ensemble has the highest mean ECS, meaning that the multi-model mean of this ensemble will likely be warmer than other scenarios multi-model mean's at the same atmospheric carbon concentration. Similarly, we were fortunate that the mean ECS of our SSP1-1.9 ensemble falls in a similar range to the other scenarios, despite it containing significantly fewer models that the other scenarios. While the impact of ensemble bias is a small effect here, the multi-model means could have had a much wider range of mean ECS values between scenario groups. In the future, any investigation using the multi-model means needs to be careful with handling the equilibrium climate sensitivity bias of the ensemble. Two ensembles constituted of differing sets of models may not always be directly comparable.

5 Conclusions

Using an ensemble of CMIP6 simulations, we have shown that the carbon allocation between Earth system components differs between scenarios after the same change in global mean surface temperature anomaly. Scenarios with higher carbon concentrations reach the global warming levels sooner, and have proportionally less carbon allocated to the ocean and land surface at that time than scenarios with lower emissions. The differences in estimated carbon emissions between scenarios vary even

at the same GWL, and can be equivalent to several years worth of global total emissions. These result appear as a result of the GWL methodology, but our conclusions are nevertheless compatible with previous works and we do not claim to refute previous target year analyses.

A model's sensitivity to CO_2 concentration significantly affects its total carbon allocation between the atmosphere, ocean and land at all global warming levels. However, our CMIP6 ensemble contains many models that fall outside the likely ECS range of 2.5 - 4. °C. By using the GWL methodology, we can exploit the full CMIP6 ensemble and weight each model equally, without excluding the so-called "hot models". We did not find a consistent relationship between ECS and any of the fractional carbon allocations. However, we did demonstrate that ECS and total carbon allocation are related. Models with lower sensitivity to carbon reach the GWL with more carbon in the individual reservoirs and more carbon overall. This is because it takes low ECS models longer to reach the same warming level, allowing more time for carbon to accumulate in the Earth system.

In addition to the impacts of ECS and total atmospheric carbon concentration, the scenario pathway also influences the carbon allocation. The SSP3-7.0 scenario includes methane induced warming and high pollution precursors cooling impacts, and the strength of these effects are model specific and not directly related to ECS. These environmental forcers in SSP3-7.0 can generate a very different warming response, GWL threshold year and carbon allocation than scenarios where CO_2, methane and pollution precursors all scale with historical values.

Ultimately, across all model simulations, a significant rise in global mean surface temperature is projected over the 21^{st} century. This underscores the need for an accelerating transition to low carbon technologies to reduce the risk of the worst effects of climate change.

Code and data availability. This analysis was performed using ESMValTool and the exact software tools used in this manuscript are available via zenodo: 10.5281/zenodo.7970638. An up-to-date version of the base ESMValTool system is available on github: github.com/ESMValGroup which includes up to date code, documentation and tutorials. CMIP6 climate model data used in this paper was obtained from the CEDA's Earth System Federation Grid node, but is widely available elsewhere: https://esgf-node.llnl.gov/search/cmip6/

Video supplement. A video abstract for this paper is available here: path-to-be-confirmed.

Author contributions. All authors contributed to the writing, discussion, initial outline, literature survey and editorial feedback of the manuscript. LdM led the work, performed the analyses and led the writing. RS, CGJ, LDM developed the GWL analysis methods. CDJ, SL, TQ contributed to the land surface carbon calculation. JW contributed to the extraction and curation of the model data. CGJ, JB, led the UKESM1 and TerraFirma projects and working groups where this work was funded.

Competing interests. The authors are not aware of any competing interests.

Acknowledgements. LdM and DIK were supported by the UK Natural Environment Research Council through The UK Earth System Modelling Project (UKESM, grant no. NE/N017951/1). RS, RJP, TQ and RPA are funded by the UK National Centre for Earth Observation (NE/N018079/1). LdM, RS, RJP, CDJ, CGJ, AY were supported by the UK Natural Environment Research Council through the TerraFIRMA: Future Impacts, Risks and Mitigation Actions in a changing Earth system project, Grant reference NE/W004895/1. CGJ acknowledges funding from the NERC National Capability UKESM grant no. NE/N017978/1 and EU Horizon 2020 project CRESCENDO, grant number: 641816. CDJ, SL and JW were supported by the Joint UK BEIS/Defra Met Office Hadley Centre Climate Programme (GA01101). CDJ was supported by the European Union's Horizon 2020 research and innovation programme under Grant Agreement No 101003536 (ESM2025 - Earth System Models for the Future). The authors would like to acknowledge use of the Centre for Environmental Data Analysis (CEDA) JASMIN computing cluster and BADC data centres in this work. The authors would also like to thank the JASMIN and ESMValTool teams for their assistance with this work.

References

Arias, P., Bellouin, N., Coppola, E., Jones, R., Krinner, G., Marotzke, J., Naik, V., Palmer, M., Plattner, G.-K., Rogelj, J., Rojas, M., Sillmann, J., Storelvmo, T., Thorne, P., Trewin, B., Achuta Rao, K., Adhikary, B., Allan, R., Armour, K., Bala, G., Barimalala, R., Berger, S., Canadell, J., Cassou, C., Cherchi, A., Collins, W., Collins, W., Connors, S., Corti, S., Cruz, F., Dentener, F., Dereczynski, C., Di Luca, A., Diongue Niang, A., Doblas-Reyes, F., Dosio, A., Douville, H., Engelbrecht, F., Eyring, V., Fischer, E., Forster, P., Fox-Kemper, B., Fuglestvedt, J., Fyfe, J., Gillett, N., Goldfarb, L., Gorodetskaya, I., Gutierrez, J., Hamdi, R., Hawkins, E., Hewitt, H., Hope, P., Islam, A., Jones, C., Kaufman, D., Kopp, R., Kosaka, Y., Kossin, J., Krakovska, S., Lee, J.-Y., Li, J., Mauritsen, T., Maycock, T., Meinshausen, M., Min, S.-K., Monteiro, P., Ngo-Duc, T., Otto, F., Pinto, I., Pirani, A., Raghavan, K., Ranasinghe, R., Ruane, A., Ruiz, L., Sallée, J.-B., Samset, B., Sathyendranath, S., Seneviratne, S., Sörensson, A., Szopa, S., Takayabu, I., Tréguier, A.-M., van den Hurk, B., Vautard, R., von Schuckmann, K., Zaehle, S., Zhang, X., and Zickfeld, K.: Technical Summary, p. 33-144, Cambridge University Press, Cambridge, United Kingdom and New York, NY, USA, https://doi.org/10.1017/9781009157896.002, 2021.

Arora, V. K., Boer, G. J., Friedlingstein, P., Eby, M., Jones, C. D., Christian, J. R., Bonan, G., Bopp, L., Brovkin, V., Cadule, P., Hajima, T., Ilyina, T., Lindsay, K., Tjiputra, J. F., and Wu, T.: Carbon–Concentration and Carbon–Climate Feedbacks in CMIP5 Earth System Models, Journal of Climate, 26, 5289 – 5314, https://doi.org/https://doi.org/10.1175/JCLI-D-12-00494.1, 2013.

Arora, V. K., Katavouta, A., Williams, R. G., Jones, C. D., Brovkin, V., Friedlingstein, P., Schwinger, J., Bopp, L., Boucher, O., Cadule, P., Chamberlain, M. A., Christian, J. R., Delire, C., Fisher, R. A., Hajima, T., Ilyina, T., Joetzjer, E., Kawamiya, M., Koven, C. D., Krasting, J. P., Law, R. M., Lawrence, D. M., Lenton, A., Lindsay, K., Pongratz, J., Raddatz, T., Séférian, R., Tachiiri, K., Tjiputra, J. F., Wiltshire, A., Wu, T., and Ziehn, T.: Carbon–concentration and carbon–climate feedbacks in CMIP6 models and their comparison to CMIP5 models, Biogeosciences, 17, 4173–4222, https://doi.org/10.5194/bg-17-4173-2020, 2020.

Bony, S., Bellon, G., Klocke, D., Sherwood, S., Fermepin, S., and Denvil, S.: Robust direct effect of carbon dioxide on tropical circulation and regional precipitation, Nature Geoscience, 6, 447–451, https://doi.org/10.1038/ngeo1799, 2013.

Boucher, O., Servonnat, J., Albright, A. L., Aumont, O., Balkanski, Y., Bastrikov, V., Bekki, S., Bonnet, R., Bony, S., Bopp, L., Braconnot, P., Brockmann, P., Cadule, P., Caubel, A., Cheruy, F., Codron, F., Cozic, A., Cugnet, D., D'Andrea, F., Davini, P., de Lavergne, C., Denvil, S., Deshayes, J., Devilliers, M., Ducharne, A., Dufresne, J.-L., Dupont, E., Éthé, C., Fairhead, L., Falletti, L., Flavoni, S., Foujols, M.-A., Gardoll, S., Gastineau, G., Ghattas, J., Grandpeix, J.-Y., Guenet, B., Guez, Lionel, E., Guilyardi, E., Guimberteau, M., Hauglustaine, D., Hourdin, F., Idelkadi, A., Joussaume, S., Kageyama, M., Khodri, M., Krinner, G., Lebas, N., Levavasseur, G., Lévy, C., Li, L., Lott, F., Lurton, T., Luyssaert, S., Madec, G., Madeleine, J.-B., Maignan, F., Marchand, M., Marti, O., Mellul, L., Meurdesoif, Y., Mignot, J., Musat, I., Ottlé, C., Peylin, P., Planton, Y., Polcher, J., Rio, C., Rochetin, N., Rousset, C., Sepulchre, P., Sima, A., Swingedouw, D., Thiéblemont, R., Traore, A. K., Vancoppenolle, M., Vial, J., Vialard, J., Viovy, N., and Vuichard, N.: Presentation and Evaluation of the IPSL-CM6A-LR Climate Model, Journal of Advances in Modeling Earth Systems, 12, e2019MS002 010, https://doi.org/https://doi.org/10.1029/2019MS002010, e2019MS002010 10.1029/2019MS002010, 2020.

Bronselaer, B., Winton, M., Russell, J., Sabine, C. L., and Khatiwala, S.: Agreement of CMIP5 Simulated and Observed Ocean Anthropogenic CO2 Uptake, Geophysical Research Letters, 44, 12,298–12,305, https://doi.org/https://doi.org/10.1002/2017GL074435, 2017.

Brunner, L., Pendergrass, A. G., Lehner, F., Merrifield, A. L., Lorenz, R., and Knutti, R.: Reduced global warming from CMIP6 projections when weighting models by performance and independence, Earth System Dynamics, 11, 995–1012, https://doi.org/10.5194/esd-11-995-2020, 2020.

Burton, C., Kelley, D. I., Jones, C. D., Betts, R. A., Cardoso, M., and Anderson, L.: South American fires and their impacts on ecosystems increase with continued emissions, Climate Resilience and Sustainability, 1, e8, https://doi.org/https://doi.org/10.1002/cli2.8, 2022.

Caesar, L., McCarthy, G. D., Thornalley, D. J. R., Cahill, N., and Rahmstorf, S.: Current Atlantic Meridional Overturning Circulation weakest in last millennium, Nature Geoscience, 14, 118–120, https://doi.org/10.1038/s41561-021-00699-z, 2021.

Caldeira, K. and Wickett, M. E.: Anthropogenic carbon and ocean pH, Nature, 425, 365–365, https://doi.org/10.1038/425365a, 2003.

Canadell, J., Monteiro, P., Costa, M., Cotrim da Cunha, L., Cox, P., Eliseev, A., Henson, S., Ishii, M., Jaccard, S., Koven, C., Lohila, A., Patra, P., Piao, S., Rogelj, J., Syampungani, S., Zaehle, S., and Zickfeld, K.: Global Carbon and other Biogeochemical Cycles and Feedbacks, p. 673–816, Cambridge University Press, Cambridge, United Kingdom and New York, NY, USA, https://doi.org/10.1017/9781009157896.007, 2021.

Christian, J. R., Denman, K. L., Hayashida, H., Holdsworth, A. M., Lee, W. G., Riche, O. G. J., Shao, A. E., Steiner, N., and Swart, N. C.: Ocean biogeochemistry in the Canadian Earth System Model version 5.0.3: CanESM5 and CanESM5-CanOE, Geoscientific Model Development, 15, 4393–4424, https://doi.org/10.5194/gmd-15-4393-2022, 2022.

Cox, P. M., Betts, R. A., Jones, C. D., Spall, S. A., and Totterdell, I. J.: Acceleration of global warming due to carbon-cycle feedbacks in a coupled climate model, Nature, 408, 184–187, https://doi.org/10.1038/35041539, 2000.

Danabasoglu, G., Lamarque, J.-F., Bacmeister, J., Bailey, D. A., DuVivier, A. K., Edwards, J., Emmons, L. K., Fasullo, J., Garcia, R., Gettelman, A., Hannay, C., Holland, M. M., Large, W. G., Lauritzen, P. H., Lawrence, D. M., Lenaerts, J. T. M., Lindsay, K., Lipscomb, W. H., Mills, M. J., Neale, R., Oleson, K. W., Otto-Bliesner, B., Phillips, A. S., Sacks, W., Tilmes, S., van Kampenhout, L., Vertenstein, M., Bertini, A., Dennis, J., Deser, C., Fischer, C., Fox-Kemper, B., Kay, J. E., Kinnison, D., Kushner, P. J., Larson, V. E., Long, M. C., Mickelson, S., Moore, J. K., Nienhouse, E., Polvani, L., Rasch, P. J., and Strand, W. G.: The Community Earth System Model Version 2 (CESM2), Journal of Advances in Modeling Earth Systems, 12, e2019MS001 916, https://doi.org/https://doi.org/10.1029/2019MS001916, e2019MS001916 2019MS001916, 2020.

Dunne, J. P., Horowitz, L. W., Adcroft, A. J., Ginoux, P., Held, I. M., John, J. G., Krasting, J. P., Malyshev, S., Naik, V., Paulot, F., Shevliakova, E., Stock, C. A., Zadeh, N., Balaji, V., Blanton, C., Dunne, K. A., Dupuis, C., Durachta, J., Dussin, R., Gauthier, P. P. G., Griffies, S. M., Guo, H., Hallberg, R. W., Harrison, M., He, J., Hurlin, W., McHugh, C., Menzel, R., Milly, P. C. D., Nikonov, S., Paynter, D. J., Ploshay, J., Radhakrishnan, A., Rand, K., Reichl, B. G., Robinson, T., Schwarzkopf, D. M., Sentman, L. T., Underwood, S., Vahlenkamp, H., Winton, M., Wittenberg, A. T., Wyman, B., Zeng, Y., and Zhao, M.: The GFDL Earth System Model Version 4.1 (GFDL-ESM 4.1): Overall Coupled Model Description and Simulation Characteristics, Journal of Advances in Modeling Earth Systems, 12, e2019MS002 015, https://doi.org/https://doi.org/10.1029/2019MS002015, e2019MS002015 2019MS002015, 2020.

Erda, L., Wei, X., Hui, J., Yinlong, X., Yue, L., Liping, B., and Liyong, X.: Climate change impacts on crop yield and quality with CO2 fertilization in China., Philos Trans R Soc Lond B Biol Sci., 360, 2149 – 2154, https://doi.org/doi/10.1098/rstb.2005.1743, 2005.

Eyring, V., Bony, S., Meehl, G. A., Senior, C. A., Stevens, B., Stouffer, R. J., and Taylor, K. E.: Overview of the Coupled Model Intercomparison Project Phase 6 (CMIP6) experimental design and organization, Geoscientific Model Development, 9, 1937–1958, https://doi.org/10.5194/gmd-9-1937-2016, 2016.

Flynn, C. M. and Mauritsen, T.: On the climate sensitivity and historical warming evolution in recent coupled model ensembles, Atmospheric Chemistry and Physics, 20, 7829–7842, https://doi.org/10.5194/acp-20-7829-2020, 2020.

Friedlingstein, P., Cox, P., Betts, R., Bopp, L., von Bloh, W., Brovkin, V., Cadule, P., Doney, S., Eby, M., Fung, I., Bala, G., John, J., Jones, C., Joos, F., Kato, T., Kawamiya, M., Knorr, W., Lindsay, K., Matthews, H. D., Raddatz, T., Rayner, P., Reick, C., Roeckner, E., Schnitzler,

K.-G., Schnur, R., Strassmann, K., Weaver, A. J., Yoshikawa, C., and Zeng, N.: Climate–Carbon Cycle Feedback Analysis: Results from the C4MIP Model Intercomparison, Journal of Climate, 19, 3337 – 3353, https://doi.org/https://doi.org/10.1175/JCLI3800.1, 2006.

Friedlingstein, P., O'Sullivan, M., Jones, M., Andrew, R., Gregor, L., Hauck, J., Le Quéré, C., Luijkx, I., Olsen, A., Peters, G., Peters, W., Pongratz, J., Schwingshackl, C., Sitch, S., Canadell, J., Ciais, P., Jackson, R., Alin, S., Alkama, R., and Zheng, B.: Global Carbon Budget 2022, Earth System Science Data, 14, 4811–4900, https://doi.org/10.5194/essd-14-4811-2022, 2022.

Friend, A. D., Lucht, W., Rademacher, T. T., Keribin, R., Betts, R., Cadule, P., Ciais, P., Clark, D. B., Dankers, R., Falloon, P. D., Ito, A., Kahana, R., Kleidon, A., Lomas, M. R., Nishina, K., Ostberg, S., Pavlick, R., Peylin, P., Schaphoff, S., Vuichard, N., Warszawski, L., Wiltshire, A., and Woodward, F. I.: Carbon residence time dominates uncertainty in terrestrial vegetation responses to future climate and atmospheric CO2, Proceedings of the National Academy of Sciences, 111, 3280–3285, https://doi.org/10.1073/pnas.1222477110, 2014.

Gjermundsen, A., Nummelin, A., Olivié, D., Bentsen, M., Seland, Ø., and Schulz, M.: Shutdown of Southern Ocean convection controls long-term greenhouse gas-induced warming, Nature Geoscience, 14, 724–731, https://doi.org/10.1038/s41561-021-00825-x, 2021.

Gregory, J. M., Ingram, W. J., Palmer, M. A., Jones, G. S., Stott, P. A., Thorpe, R. B., Lowe, J. A., Johns, T. C., and Williams, K. D.: A new method for diagnosing radiative forcing and climate sensitivity, Geophysical Research Letters, 31, https://doi.org/https://doi.org/10.1029/2003GL018747, 2004.

Hajima, T., Watanabe, M., Yamamoto, A., Tatebe, H., Noguchi, M. A., Abe, M., Ohgaito, R., Ito, A., Yamazaki, D., Okajima, H., Ito, A., Takata, K., Ogochi, K., Watanabe, S., and Kawamiya, M.: Development of the MIROC-ES2L Earth system model and the evaluation of biogeochemical processes and feedbacks, Geoscientific Model Development, 13, 2197–2244, https://doi.org/10.5194/gmd-13-2197-2020, 2020.

Hansen, J., Johnson, D., Lacis, A., Lebedeff, S., Lee, P., Rind, D., and Russell, G.: Climate Impact of Increasing Atmospheric Carbon Dioxide, Science, 213, 957–966, https://doi.org/10.1126/science.213.4511.957, 1981.

Hauck, J., Zeising, M., Le Quéré, C., Gruber, N., Bakker, D. C. E., Bopp, L., Chau, T. T. T., G urses, O., Ilyina, T., Landschützer, P., Lenton, A., Resplandy, L., Rödenbeck, C., Schwinger, J., and Séférian, R.: Consistency and Challenges in the Ocean Carbon Sink Estimate for the Global Carbon Budget, Frontiers in Marine Science, 7, https://doi.org/10.3389/fmars.2020.571720, 2020.

Hausfather, Z., Marvel, K., Schmidt, G. A., Nielsen-Gammon, J. W., and Zelinka, M.: Climate simulations: Recognize the 'hot model' problem, Nature, 605, 26–29, https://doi.org/10.1038/d41586-022-01192-2, 2022.

Hilmi, N., Chami, R., Sutherland, M. D., Hall-Spencer, J. M., Lebleu, L., Benitez, M. B., and Levin, L. A.: The Role of Blue Carbon in Climate Change Mitigation and Carbon Stock Conservation, Frontiers in Climate, 3, https://doi.org/10.3389/fclim.2021.710546, 2021.

IPCC: Climate Change 2021: The Physical Science Basis. Contribution of Working Group I to the Sixth Assessment Report of the Intergovernmental Panel on Climate Change, vol. In Press, Cambridge University Press, Cambridge, United Kingdom and New York, NY, USA, https://doi.org/10.1017/9781009157896, 2021a.

IPCC: Summary for Policymakers, p. 3-32, Cambridge University Press, Cambridge, United Kingdom and New York, NY, USA, https://doi.org/10.1017/9781009157896.001, 2021b.

Jacobson, A. R., Mikaloff Fletcher, S. E., Gruber, N., Sarmiento, J. L., and Gloor, M.: A joint atmosphere-ocean inversion for surface fluxes of carbon dioxide: 2. Regional results, Global Biogeochemical Cycles, 21, https://doi.org/https://doi.org/10.1029/2006GB002703, 2007.

Jiang, L., Yan, Y., Hararuk, O., Mikle, N., Xia, J., Shi, Z., Tjiputra, J., Wu, T., and Luo, Y.: Scale-Dependent Performance of CMIP5 Earth System Models in Simulating Terrestrial Vegetation Carbon, Journal of Climate, 28, 5217 – 5232, https://doi.org/https://doi.org/10.1175/JCLI-D-14-00270.1, 2015.

Jiang, L., Liang, J., Lu, X., Hou, E., Hoffman, F. M., and Luo, Y.: Country-level land carbon sink and its causing components by the middle of the twenty-first century, Ecological Processes, 10, 61, https://doi.org/10.1186/s13717-021-00328-y, 2021.

Jiang, L.-Q., Carter, B. R., Feely, R. A., Lauvset, S. K., and Olsen, A.: Surface ocean pH and buffer capacity: past, present and future, Scientific Reports, 9, 18 624, https://doi.org/10.1038/s41598-019-55039-4, 2019.

Jones, C., Robertson, E., Arora, V., Friedlingstein, P., Shevliakova, E., Bopp, L., Brovkin, V., Hajima, T., Kato, E., Kawamiya, M., Liddicoat, S., Lindsay, K., Reick, C. H., Roelandt, C., Segschneider, J., and Tjiputra, J.: Twenty-First-Century Compatible CO2 Emissions and Airborne Fraction Simulated by CMIP5 Earth System Models under Four Representative Concentration Pathways, Journal of Climate, 26, 4398 – 4413, https://doi.org/10.1175/JCLI-D-12-00554.1, 2013.

Jones, C. D., Hughes, J. K., Bellouin, N., Hardiman, S. C., Jones, G. S., Knight, J., Liddicoat, S., O'Connor, F. M., Andres, R. J., Bell, C., Boo, K.-O., Bozzo, A., Butchart, N., Cadule, P., Corbin, K. D., Doutriaux-Boucher, M., Friedlingstein, P., Gornall, J., Gray, L., Halloran, P. R., Hurtt, G., Ingram, W. J., Lamarque, J.-F., Law, R. M., Meinshausen, M., Osprey, S., Palin, E. J., Parsons Chini, L., Raddatz, T., Sanderson, M. G., Sellar, A. A., Schurer, A., Valdes, P., Wood, N., Woodward, S., Yoshioka, M., and Zerroukat, M.: The HadGEM2-ES implementation of CMIP5 centennial simulations, Geoscientific Model Development, 4, 543–570, https://doi.org/10.5194/gmd-4-543-2011, 2011.

Jones, C. D., Arora, V., Friedlingstein, P., Bopp, L., Brovkin, V., Dunne, J., Graven, H., Hoffman, F., Ilyina, T., John, J. G., Jung, M., Kawamiya, M., Koven, C., Pongratz, J., Raddatz, T., Randerson, J. T., and Zaehle, S.: C4MIP – The Coupled Climate–Carbon Cycle Model Intercomparison Project: experimental protocol for CMIP6, Geoscientific Model Development, 9, 2853–2880, https://doi.org/10.5194/gmd-9-2853-2016, 2016.

Katavouta, A. and Williams, R. G.: Ocean carbon cycle feedbacks in CMIP6 models: contributions from different basins, Biogeosciences, 18, 3189–3218, https://doi.org/10.5194/bg-18-3189-2021, 2021.

Koch, A., Hubau, W., and Lewis, S. L.: Earth System Models Are Not Capturing Present-Day Tropical Forest Carbon Dynamics, Earth's Future, 9, e2020EF001 874, https://doi.org/https://doi.org/10.1029/2020EF001874, e2020EF001874 2020EF001874, 2021.

Kroeker, K. J., Kordas, R. L., Crim, R., Hendriks, I. E., Ramajo, L., Singh, G. S., Duarte, C. M., and Gattuso, J.-P.: Impacts of ocean acidification on marine organisms: quantifying sensitivities and interaction with warming, Global Change Biology, 19, 1884–1896, https://doi.org/https://doi.org/10.1111/gcb.12179, 2013.

Lawrence, M. G., Schäfer, S., Muri, H., Scott, V., Oschlies, A., Vaughan, N. E., Boucher, O., Schmidt, H., Haywood, J., and Scheffran, J.: Evaluating climate geoengineering proposals in the context of the Paris Agreement temperature goals, Nature Communications, 9, 3734, https://doi.org/10.1038/s41467-018-05938-3, 2018.

Le Quéré, C., Andrew, R. M., Friedlingstein, P., Sitch, S., Hauck, J., Pongratz, J., Pickers, P. A., Korsbakken, J. I., Peters, G. P., Canadell, J. G., Arneth, A., Arora, V. K., Barbero, L., Bastos, A., Bopp, L., Chevallier, F., Chini, L. P., Ciais, P., Doney, S. C., Gkritzalis, T., Goll, D. S., Harris, I., Haverd, V., Hoffman, F. M., Hoppema, M., Houghton, R. A., Hurtt, G., Ilyina, T., Jain, A. K., Johannessen, T., Jones, C. D., Kato, E., Keeling, R. F., Goldewijk, K. K., Landschützer, P., Lefèvre, N., Lienert, S., Liu, Z., Lombardozzi, D., Metzl, N., Munro, D. R., Nabel, J. E. M. S., Nakaoka, S., Neill, C., Olsen, A., Ono, T., Patra, P., Peregon, A., Peters, W., Peylin, P., Pfeil, B., Pierrot, D., Poulter, B., Rehder, G., Resplandy, L., Robertson, E., Rocher, M., Rödenbeck, C., Schuster, U., Schwinger, J., Séférian, R., Skjelvan, I., Steinhoff, T., Sutton, A., Tans, P. P., Tian, H., Tilbrook, B., Tubiello, F. N., van der Laan-Luijkx, I. T., van der Werf, G. R., Viovy, N., Walker, A. P., Wiltshire, A. J., Wright, R., Zaehle, S., and Zheng, B.: Global Carbon Budget 2018, Earth System Science Data, 10, 2141–2194, https://doi.org/10.5194/essd-10-2141-2018, 2018.

Lee, J.-Y., Marotzke, J., Bala, G., Cao, L., Corti, S., Dunne, J., Engelbrecht, F., Fischer, E., Fyfe, J., Jones, C., Maycock, A., Mutemi, J., Ndiaye, O., Panickal, S., and Zhou, T.: Future Global Climate: Scenario-Based Projections and Near-Term Information, p. 553–672, Cambridge University Press, Cambridge, United Kingdom and New York, NY, USA, https://doi.org/10.1017/9781009157896.006, 2021.

Li, G., Cheng, L., Zhu, J., Trenberth, K. E., Mann, M. E., and Abraham, J. P.: Increasing ocean stratification over the past half-century, Nature Climate Change, 10, 1116–1123, https://doi.org/10.1038/s41558-020-00918-2, 2020.

Liddicoat, S. K., Wiltshire, A. J., Jones, C. D., Arora, V. K., Brovkin, V., Cadule, P., Hajima, T., Lawrence, D. M., Pongratz, J., Schwinger, J., Séférian, R., Tjiputra, J. F., and Ziehn, T.: Compatible Fossil Fuel CO2 Emissions in the CMIP6 Earth System Models' Historical and Shared Socioeconomic Pathway Experiments of the Twenty-First Century, Journal of Climate, 34, 2853 – 2875, https://doi.org/10.1175/JCLI-D-19-0991.1, 2021.

Lovato, T., Peano, D., Butenschön, M., Materia, S., Iovino, D., Scoccimarro, E., Fogli, P. G., Cherchi, A., Bellucci, A., Gualdi, S., Masina, S., and Navarra, A.: CMIP6 Simulations With the CMCC Earth System Model (CMCC-ESM2), Journal of Advances in Modeling Earth Systems, 14, e2021MS002 814, https://doi.org/https://doi.org/10.1029/2021MS002814, e2021MS002814 2021MS002814, 2022a.

Lovato, T., Peano, D., Butenschön, M., Materia, S., Iovino, D., Scoccimarro, E., Fogli, P. G., Cherchi, A., Bellucci, A., Gualdi, S., Masina, S., and Navarra, A.: CMIP6 Simulations With the CMCC Earth System Model (CMCC-ESM2), Journal of Advances in Modeling Earth Systems, 14, e2021MS002 814, https://doi.org/https://doi.org/10.1029/2021MS002814, e2021MS002814 2021MS002814, 2022b.

Macreadie, P. I., Anton, A., Raven, J. A., Beaumont, N., Connolly, R. M., Friess, D. A., Kelleway, J. J., Kennedy, H., Kuwae, T., Lavery, P. S., Lovelock, C. E., Smale, D. A., Apostolaki, E. T., Atwood, T. B., Baldock, J., Bianchi, T. S., Chmura, G. L., Eyre, B. D., Fourqurean, J. W., Hall-Spencer, J. M., Huxham, M., Hendriks, I. E., Krause-Jensen, D., Laffoley, D., Luisetti, T., Marbà, N., Masque, P., McGlathery, K. J., Megonigal, J. P., Murdiyarso, D., Russell, B. D., Santos, R., Serrano, O., Silliman, B. R., Watanabe, K., and Duarte, C. M.: The future of Blue Carbon science, Nature Communications, 10, 3998, https://doi.org/10.1038/s41467-019-11693-w, 2019.

Mauritsen, T., Bader, J., Becker, T., Behrens, J., Bittner, M., Brokopf, R., Brovkin, V., Claussen, M., Crueger, T., Esch, M., Fast, I., Fiedler, S., Fläschner, D., Gayler, V., Giorgetta, M., Goll, D. S., Haak, H., Hagemann, S., Hedemann, C., Hohenegger, C., Ilyina, T., Jahns, T., Jimenéz-de-la Cuesta, D., Jungclaus, J., Kleinen, T., Kloster, S., Kracher, D., Kinne, S., Kleberg, D., Lasslop, G., Kornblueh, L., Marotzke, J., Matei, D., Meraner, K., Mikolajewicz, U., Modali, K., Möbis, B., Müller, W. A., Nabel, J. E. M. S., Nam, C. C. W., Notz, D., Nyawira, S.-S., Paulsen, H., Peters, K., Pincus, R., Pohlmann, H., Pongratz, J., Popp, M., Raddatz, T. J., Rast, S., Redler, R., Reick, C. H., Rohrschneider, T., Schemann, V., Schmidt, H., Schnur, R., Schulzweida, U., Six, K. D., Stein, L., Stemmler, I., Stevens, B., von Storch, J.-S., Tian, F., Voigt, A., Vrese, P., Wieners, K.-H., Wilkenskjeld, S., Winkler, A., and Roeckner, E.: Developments in the MPI-M Earth System Model version 1.2 (MPI-ESM1.2) and Its Response to Increasing CO2, Journal of Advances in Modeling Earth Systems, 11, 998–1038, https://doi.org/https://doi.org/10.1029/2018MS001400, 2019.

Meehl, G. A., Senior, C. A., Eyring, V., Flato, G., Lamarque, J.-F., Stouffer, R. J., Taylor, K. E., and Schlund, M.: Context for interpreting equilibrium climate sensitivity and transient climate response from the CMIP6 Earth system models, Science Advances, 6, eaba1981, https://doi.org/10.1126/sciadv.aba1981, 2020.

Meinshausen, M., Vogel, E., Nauels, A., Lorbacher, K., Meinshausen, N., Etheridge, D. M., Fraser, P. J., Montzka, S. A., Rayner, P. J., Trudinger, C. M., Krummel, P. B., Beyerle, U., Canadell, J. G., Daniel, J. S., Enting, I. G., Law, R. M., Lunder, C. R., O'Doherty, S., Prinn, R. G., Reimann, S., Rubino, M., Velders, G. J. M., Vollmer, M. K., Wang, R. H. J., and Weiss, R.: Historical greenhouse gas concentrations for climate modelling (CMIP6), Geoscientific Model Development, 10, 2057–2116, https://doi.org/10.5194/gmd-10-2057-2017, 2017.

Meinshausen, M., Nicholls, Z. R. J., Lewis, J., Gidden, M. J., Vogel, E., Freund, M., Beyerle, U., Gessner, C., Nauels, A., Bauer, N., Canadell, J. G., Daniel, J. S., John, A., Krummel, P. B., Luderer, G., Meinshausen, N., Montzka, S. A., Rayner, P. J., Reimann, S., Smith, S. J., van den Berg, M., Velders, G. J. M., Vollmer, M. K., and Wang, R. H. J.: The shared socio-economic pathway (SSP) greenhouse gas concentrations and their extensions to 2500, Geoscientific Model Development, 13, 3571–3605, https://doi.org/10.5194/gmd-13-3571-2020, 2020.

Muilwijk, M., Nummelin, A., Heuzé, C., Polyakov, I. V., Zanowski, H., and Smedsrud, L. H.: Divergence in Climate Model Projections of Future Arctic Atlantification, Journal of Climate, 36, 1727 – 1748, https://doi.org/https://doi.org/10.1175/JCLI-D-22-0349.1, 2023.

Myers, N.: Carbon Dioxide Review, Environmental Conservation, 10, 370–371, https://doi.org/10.1017/S0376892900013345, 1983.

Nyberg, M. and Hovenden, M. J.: Warming increases soil respiration in a carbon-rich soil without changing microbial respiratory potential, Biogeosciences, 17, 4405–4420, https://doi.org/10.5194/bg-17-4405-2020, 2020.

O'Neill, B. C., Tebaldi, C., van Vuuren, D. P., Eyring, V., Friedlingstein, P., Hurtt, G., Knutti, R., Kriegler, E., Lamarque, J.-F., Lowe, J., Meehl, G. A., Moss, R., Riahi, K., and Sanderson, B. M.: The Scenario Model Intercomparison Project (ScenarioMIP) for CMIP6, Geoscientific Model Development, 9, 3461–3482, https://doi.org/10.5194/gmd-9-3461-2016, 2016.

Pongratz, J., Reick, C. H., Houghton, R. A., and House, J. I.: Terminology as a key uncertainty in net land use and land cover change carbon flux estimates, Earth System Dynamics, 5, 177–195, https://doi.org/10.5194/esd-5-177-2014, 2014.

Raupach, M. R., Gloor, M., Sarmiento, J. L., Canadell, J. G., Frölicher, T. L., Gasser, T., Houghton, R. A., Le Quéré, C., and Trudinger, C. M.: The declining uptake rate of atmospheric CO_2 by land and ocean sinks, Biogeosciences, 11, 3453–3475, https://doi.org/10.5194/bg-11-3453-2014, 2014.

Resplandy, L., Keeling, R., Rödenbeck, C., Stephens, B. B., Khatiwala, S., Rodgers, K., Long, M. C., Bopp, L., and Tans, P. P.: Revision of global carbon fluxes based on a reassessment of oceanic and riverine carbon transport, Nature Geoscience, 11, 504—509, https://doi.org/10.1038/s41561-018-0151-3, 2018.

Riahi, K., van Vuuren, D. P., Kriegler, E., Edmonds, J., O'Neill, B. C., Fujimori, S., Bauer, N., Calvin, K., Dellink, R., Fricko, O., Lutz, W., Popp, A., Cuaresma, J. C., KC, S., Leimbach, M., Jiang, L., Kram, T., Rao, S., Emmerling, J., Ebi, K., Hasegawa, T., Havlik, P., Humpenöder, F., Da Silva, L. A., Smith, S., Stehfest, E., Bosetti, V., Eom, J., Gernaat, D., Masui, T., Rogelj, J., Strefler, J., Drouet, L., Krey, V., Luderer, G., Harmsen, M., Takahashi, K., Baumstark, L., Doelman, J. C., Kainuma, M., Klimont, Z., Marangoni, G., Lotze-Campen, H., Obersteiner, M., Tabeau, A., and Tavoni, M.: The Shared Socioeconomic Pathways and their energy, land use, and greenhouse gas emissions implications: An overview, Global Environmental Change, 42, 153–168, https://doi.org/https://doi.org/10.1016/j.gloenvcha.2016.05.009, 2017.

Righi, M., Andela, B., Eyring, V., Lauer, A., Predoi, V., Schlund, M., Vegas-Regidor, J., Bock, L., Brötz, B., de Mora, L., Diblen, F., Dreyer, L., Drost, N., Earnshaw, P., Hassler, B., Koldunov, N., Little, B., Loosveldt Tomas, S., and Zimmermann, K.: Earth System Model Evaluation Tool (ESMValTool) v2.0 – technical overview, Geoscientific Model Development, 13, 1179–1199, https://doi.org/10.5194/gmd-13-1179-2020, 2020.

Roser, M. and Ritchie, H.: Oil Spills, Our World in Data, https://ourworldindata.org/oil-spills, 2022.

Sallée, J.-B., Pellichero, V., Akhoudas, C., Pauthenet, E., Vignes, L., Schmidtko, S., Garabato, A. N., Sutherland, P., and Kuusela, M.: Summertime increases in upper-ocean stratification and mixed-layer depth, Nature, 591, 592–598, https://doi.org/10.1038/s41586-021-03303-x, 2021.

Scafetta, N.: Advanced Testing of Low, Medium, and High ECS CMIP6 GCM Simulations Versus ERA5-T2m, Geophysical Research Letters, 49, e2022GL097 716, https://doi.org/https://doi.org/10.1029/2022GL097716, e2022GL097716 2022GL097716, 2022.

Schlunegger, S., Rodgers, K. B., Sarmiento, J. L., Frölicher, T. L., Dunne, J. P., Ishii, M., and Slater, R.: Emergence of anthropogenic signals in the ocean carbon cycle, Nature Climate Change, 9, 719–725, https://doi.org/10.1038/s41558-019-0553-2, 2019.

Sellar, A. A., Walton, J., Jones, C. G., Wood, R., Abraham, N. L., Andrejczuk, M., Andrews, M. B., Andrews, T., Archibald, A. T., de Mora, L., Dyson, H., Elkington, M., Ellis, R., Florek, P., Good, P., Gohar, L., Haddad, S., Hardiman, S. C., Hogan, E., Iwi, A., Jones, C. D., Johnson, B., Kelley, D. I., Kettleborough, J., Knight, J. R., Köhler, M. O., Kuhlbrodt, T., Liddicoat, S., Linova-Pavlova, I., Mizielinski, M. S., Morgenstern, O., Mulcahy, J., Neininger, E., O'Connor, F. M., Petrie, R., Ridley, J., Rioual, J.-C., Roberts, M., Robertson, E., Rumbold, S., Seddon, J., Shepherd, H., Shim, S., Stephens, A., Teixiera, J. C., Tang, Y., Williams, J., Wiltshire, A., and Griffiths, P. T.: Implementation of U.K. Earth System Models for CMIP6, Journal of Advances in Modeling Earth Systems, 12, e2019MS001 946, https://doi.org/https://doi.org/10.1029/2019MS001946, e2019MS001946 10.1029/2019MS001946, 2020.

Sherwood, S. C., Webb, M. J., Annan, J. D., Armour, K. C., Forster, P. M., Hargreaves, J. C., Hegerl, G., Klein, S. A., Marvel, K. D., Rohling, E. J., Watanabe, M., Andrews, T., Braconnot, P., Bretherton, C. S., Foster, G. L., Hausfather, Z., von der Heydt, A. S., Knutti, R., Mauritsen, T., Norris, J. R., Proistosescu, C., Rugenstein, M., Schmidt, G. A., Tokarska, K. B., and Zelinka, M. D.: An Assessment of Earth's Climate Sensitivity Using Multiple Lines of Evidence, Reviews of Geophysics, 58, e2019RG000 678, https://doi.org/https://doi.org/10.1029/2019RG000678, e2019RG000678 2019RG000678, 2020.

Sullivan, A., Baker, E., and Kurvits, T.: Spreading Like Wildfire: The Rising Threat of Extraordinary Landscape Fires, Tech. rep., UN Environment Program, https://policycommons.net/artifacts/2259313/wildfire_rra/, 2022.

Swaminathan, R., Parker, R. J., Jones, C. G., Allan, R. P., Quaife, T., Kelley, D. I., de Mora, L., and Walton, J.: The Physical Climate at Global Warming Thresholds as Seen in the U.K. Earth System Model, Journal of Climate, 35, 29 – 48, https://doi.org/10.1175/JCLI-D-21-0234.1, 2022.

Swart, N. C., Cole, J. N. S., Kharin, V. V., Lazare, M., Scinocca, J. F., Gillett, N. P., Anstey, J., Arora, V., Christian, J. R., Hanna, S., Jiao, Y., Lee, W. G., Majaess, F., Saenko, O. A., Seiler, C., Seinen, C., Shao, A., Sigmond, M., Solheim, L., von Salzen, K., Yang, D., and Winter, B.: The Canadian Earth System Model version 5 (CanESM5.0.3), Geoscientific Model Development, 12, 4823–4873, https://doi.org/10.5194/gmd-12-4823-2019, 2019.

Tebaldi, C., Debeire, K., Eyring, V., Fischer, E., Fyfe, J., Friedlingstein, P., Knutti, R., Lowe, J., O'Neill, B., Sanderson, B., van Vuuren, D., Riahi, K., Meinshausen, M., Nicholls, Z., Tokarska, K. B., Hurtt, G., Kriegler, E., Lamarque, J.-F., Meehl, G., Moss, R., Bauer, S. E., Boucher, O., Brovkin, V., Byun, Y.-H., Dix, M., Gualdi, S., Guo, H., John, J. G., Kharin, S., Kim, Y., Koshiro, T., Ma, L., Olivié, D., Panickal, S., Qiao, F., Rong, X., Rosenbloom, N., Schupfner, M., Séférian, R., Sellar, A., Semmler, T., Shi, X., Song, Z., Steger, C., Stouffer, R., Swart, N., Tachiiri, K., Tang, Q., Tatebe, H., Voldoire, A., Volodin, E., Wyser, K., Xin, X., Yang, S., Yu, Y., and Ziehn, T.: Climate model projections from the Scenario Model Intercomparison Project (ScenarioMIP) of CMIP6, Earth System Dynamics, 12, 253–293, https://doi.org/10.5194/esd-12-253-2021, 2021.

Thibodeau, B., Not, C., Zhu, J., Schmittner, A., Noone, D., Tabor, C., Zhang, J., and Liu, Z.: Last Century Warming Over the Canadian Atlantic Shelves Linked to Weak Atlantic Meridional Overturning Circulation, Geophysical Research Letters, 45, 12,376–12,385, https://doi.org/https://doi.org/10.1029/2018GL080083, 2018.

Twomey, S.: The Influence of Pollution on the Shortwave Albedo of Clouds, Journal of Atmospheric Sciences, 34, 1149 – 1152, https://doi.org/10.1175/1520-0469(1977)034<1149:TIOPOT>2.0.CO;2, 1977.

Ukkola, A. M., Prentice, I., Keenan, T. F., van Dijk, A. I., Viney, N. R., Myneni, R., and Bi, J.: Reduced streamflow in water-stressed climates consistent with CO2 effects on vegetation, Nature Climate Change, 6, 75–78, https://doi.org/10.1038/nclimate2831, 2016.

United Nations: Transforming our world : the 2030 Agenda for Sustainable Development : resolution /, p. 35 p., http://digitallibrary.un.org/record/3923923, issued in GAOR, 70th sess., Suppl. no. 49., 2015.

United Nations Environment Programme: Emissions Gap Report 2019, https://wedocs.unep.org/20.500.11822/30797, 2019.

United Nations Treaty Collection: Paris Agreement, https://treaties.un.org/pages/ViewDetails.aspx?src=TREATY&mtdsg_no=XXVII-7-d&chapter=27&clang=_en, 2015.

Wang, S., Zhang, Y., Ju, W., Chen, J. M., Ciais, P., Cescatti, A., Sardans, J., Janssens, I. A., Wu, M., Berry, J. A., Campbell, E., Fernández-Martínez, M., Alkama, R., Sitch, S., Friedlingstein, P., Smith, W. K., Yuan, W., He, W., Lombardozzi, D., Kautz, M., Zhu, D., Lienert, S., Kato, E., Poulter, B., Sanders, T. G. M., Krüger, I., Wang, R., Zeng, N., Tian, H., Vuichard, N., Jain, A. K., Wiltshire, A., Haverd, V., Goll, D. S., and Peñuelas, J.: Recent global decline of CO2 fertilization effects on vegetation photosynthesis, Science, 370, 1295–1300, https://doi.org/10.1126/science.abb7772, 2020.

Watson, A. J., Schuster, U., Shutler, J. D., Holding, T., Ashton, I. G. C., Landschützer, P., Woolf, D. K., and Goddijn-Murphy, L.: Revised estimates of ocean-atmosphere CO2 flux are consistent with ocean carbon inventory, Nature Communications, 11, 4422, https://doi.org/10.1038/s41467-020-18203-3, 2020.

Weijer, W., Cheng, W., Garuba, O. A., Hu, A., and Nadiga, B. T.: CMIP6 Models Predict Significant 21st Century Decline of the Atlantic Meridional Overturning Circulation, Geophysical Research Letters, 47, e2019GL086 075, https://doi.org/https://doi.org/10.1029/2019GL086075, e2019GL086075 10.1029/2019GL086075, 2020.

Yool, A., Palmiéri, J., Jones, C. G., Sellar, A. A., de Mora, L., Kuhlbrodt, T., Popova, E. E., Mulcahy, J. P., Wiltshire, A., Rumbold, S. T., Stringer, M., Hill, R. S. R., Tang, Y., Walton, J., Blaker, A., Nurser, A. J. G., Coward, A. C., Hirschi, J., Woodward, S., Kelley, D. I., Ellis, R., and Rumbold-Jones, S.: Spin-up of UK Earth System Model 1 (UKESM1) for CMIP6, Journal of Advances in Modeling Earth Systems, 12, e2019MS001 933, https://doi.org/https://doi.org/10.1029/2019MS001933, e2019MS001933 10.1029/2019MS001933, 2020.

Zeebe, R. E.: History of Seawater Carbonate Chemistry, Atmospheric CO2, and Ocean Acidification, Annual Review of Earth and Planetary Sciences, 40, 141–165, https://doi.org/10.1146/annurev-earth-042711-105521, 2012.

Zelinka, M. D., Myers, T. A., McCoy, D. T., Po-Chedley, S., Caldwell, P. M., Ceppi, P., Klein, S. A., and Taylor, K. E.: Causes of Higher Climate Sensitivity in CMIP6 Models, Geophysical Research Letters, 47, e2019GL085 782, https://doi.org/https://doi.org/10.1029/2019GL085782, e2019GL085782 10.1029/2019GL085782, 2020.

Ziehn, T., Chamberlain, M. A., Law, R. M., Lenton, A., Bodman, R. W., Dix, M., Stevens, L., Wang, Y.-P., and Srbinovsky, J.: The Australian Earth System Model: ACCESS-ESM1.5, Journal of Southern Hemisphere Earth Systems Science, 70, 193–214, https://doi.org/10.1071/ES19035, 2020.

Ågren, G. I., Wetterstedt, J. A. M., and Billberger, M. F. K.: Nutrient limitation on terrestrial plant growth – modeling the interaction between nitrogen and phosphorus, New Phytologist, 194, 953–960, https://doi.org/https://doi.org/10.1111/j.1469-8137.2012.04116.x, 2012.